Electronic Supplementary Material (ESI) for Physical Chemistry Chemical Physics.

Supplementary Information

Single Atom Alloy vs Phase Separated Alloy in Cu, Ag, and Au atoms with Ni(111) and Ni, Pd, and Pt atoms with Cu(111): Theoretical Exploration

Junqing Yin,[†] Masahiro Ehara,[†, ‡] and Shigeyoshi Sakaki[†*]

[†] Elements Strategy Initiative for Catalysts and Batteries (ESICB), Kyoto University, Goryo-Ohara 1-30, Nishikyo-ku, Kyoto 615-8245, Japan

[‡] Institute for Molecular Science (IMS), Okazaki 444-8585, Japan

Corresponding Author

E-mails: sakaki.shigeyoshi.47e@st.kyoto-u.ac.jp. Phone: +81-75-383-3036

Table of Contents

1. Effects of D3 correction on the CO adsorption and the relative energies of alloys.

Table S1. Influences of D3 correction on the C-O and M-C distances ($d_{C\text{-}O}$ and $d_{M\text{-}C}$ in Å) of CO adsorbed at the hollow site on the M(111) surfaces (M = Ni, Cu)

CO at H site	$d_{C\text{-}O}$		$d_{M\text{-}C}$	
	PBE	PBE + D3(BJ)	PBE	PBE + D3(BJ)
Ni(111)	1.196	1.195	1.948 / 1.946 / 1.946	1.943 / 1.943 / 1.943
Cu(111)	1.185	1.184	2.045 / 2.046 / 2.045	2.043 / 2.041 / 2.041

Table S2. Influences of D3 correction on relative energies of the SAA and PSA, where the 2Cu/Ni(111) and 3Cu/Ni(111) were calculated as examples.

nCu/Ni(111)		RE / eV	
		PBE	PBE+D3(BJ)
2Cu/Ni(111)	SAA_2Cu_1	0	0
	SAA_2Cu_2	0.020	0.019
	PSA_2Cu	-0.013	-0.014
3Cu/Ni(111)	SAA_3Cu_1	0	0.000
	SAA_3Cu_2	0.060	0.057
	PSA_3Cu_C	-0.032	-0.035
	PSA_3Cu_L	-0.023	-0.025

2. Geometries and relative stabilities of nX/M(111) alloy with X at the surface and the inside

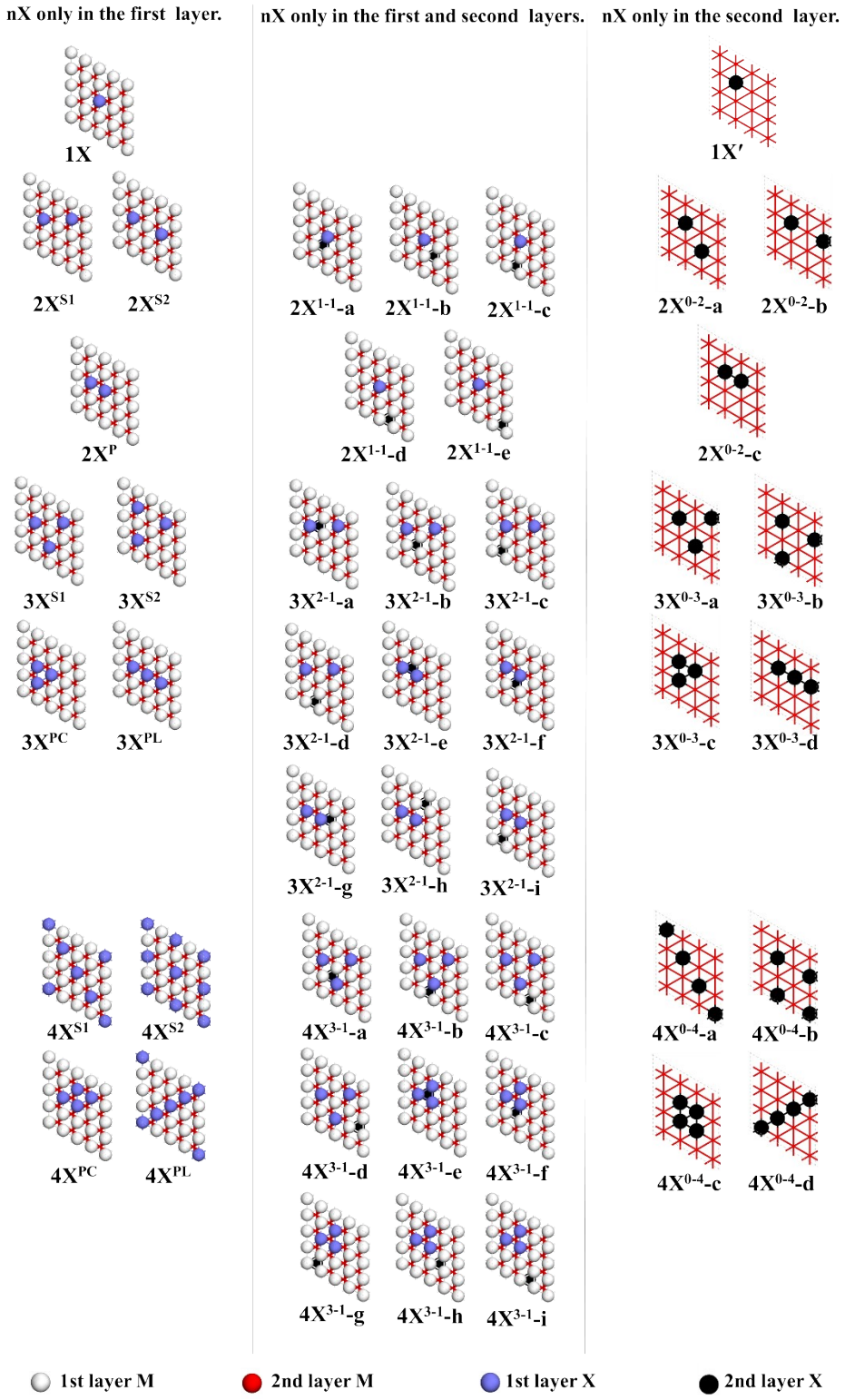

Scheme S1. Geometries of nX/M(111) (n = 1 ~ 4) with nX atoms in the first and/or second layers.

Table S3. Relative energies (ΔE in eV) of the nX/M(111) (n = 1 ~ 4) alloys geometries in Scheme S2. The ΔE is calculated with the total energy of the most stable SAA structure as reference.

Distribution of nX atoms			nX/Ni(111)			nX/Cu(111)		
			X = Cu	X = Ag	X = Au	X = Ni	X = Pd	X = Pt
n = 1	1st-layer	1X	0	0	0	0	0	0
	2nd-layer	1X′	0.238	1.114	1.112	-0.199	0.166	0.183
n = 2	1st-layer	$2X^{S1}$	0	0	0	0	0	0.007
		$2X^{S2}$	0.020	0.070	0.055	0.008	0.019	0
		$2X^{P}$	–0.013	0.003	0.086	0.006	0.084	0.123
		2a	0.210	0.833	0.971	-0.186	0.245	0.368
	1st+2nd layer2	2b	0.240	1.072	1.062	-0.185	0.154	0.194
		2c	0.231	1.090	1.116	-0.187	0.183	0.193
		2d	0.235	1.068	1.117	-0.197	0.169	0.186
		2e	0.235	1.068	1.117	-0.197	0.169	0.186
	2nd-layer	$2X^{S1'}$	0.468	2.206	2.279	-0.377	0.367	0.404
		$2X^{S2'}$	0.462	2.267	2.343	-0.391	0.351	0.356
		$2X^{P'}$	0.456	2.131	2.342	-0.369	0.432	0.526
n = 3	1st-layer	$3X^{S1}$	0	0	0	0	0	0.028
		$3X^{S2}$	0.06	0.174	0.128	0.021	0.051	0
		$3X^{PC}$	–0.032	–0.009	0.188	0.003	0.213	0.314
		$3X^{PL}$	–0.023	0.071	0.281	0.023	0.229	0.304
	1st+2nd layers	3a	0.221	0.790	0.849	-0.179	0.218	0.373
		3b	0.237	1.052	1.009	-0.177	0.163	0.212
		3c	0.227	1.054	1.050	-0.187	0.179	0.205
		3d	0.247	1.065	1.075	-0.201	0.148	0.181
		3e	0.170	0.541	0.844	-0.190	0.369	0.590
		3f	0.202	0.780	0.929	-0.172	0.307	0.496
		3g	0.196	0.790	0.968	-0.181	0.333	0.493
		3h	0.226	1.043	1.084	-0.172	0.243	0.327
		3i	0.216	1.049	1.128	-0.189	0.241	0.299

		3j	0.220	1.046	1.140	-0.179	0.247	0.373
	2^{nd}-layer	$3X^{S1'}$	0.697	3.312	3.396	-0.544	0.586	0.656
		$3X^{S2'}$	0.683	3.474	3.561	-0.583	0.537	0.515
		$3X^{PC'}$	0.668	3.090	3.538	-0.549	0.709	0.907
		$3X^{PL'}$	0.654	3.181	3.621	-0.540	0.719	0.900
n = 4	1^{st}-layer	$4X^{S1}$	0	0	0	0	0	0.038
		$4X^{S2}$	0.071	0.206	0.156	0.028	0.061	0
		$4X^{PC}$	-0.109	-0.132	0.229	-0.022	0.328	0.523
		$4X^{PL}$	-0.113	0.163	0.761	0.046	0.517	0.752
	1^{st}+2^{nd} layers	4a	0.168	0.688	0.738	-0.190	0.179	0.391
		4b	0.175	0.663	0.780	-0.185	0.126	0.232
		4c	0.189	0.914	0.885	-0.211	0.170	0.368
		4d	0.190	0.914	0.885	-0.194	0.115	0.229
		4e	0.076	0.088	0.661	-0.233	0.478	0.825
		4f	0.137	0.627	0.882	-0.191	0.398	0.687
		4g	0.164	0.933	1.121	-0.201	0.337	0.496
		4h	0.165	0.891	1.079	-0.199	0.319	0.529
		4i	0.165	0.893	1.082	-0.199	0.319	0.528
	2^{nd}-layer	$4X^{S1'}$	0.869	4.235	4.483	-0.731	0.810	1.019
		$4X^{S2'}$	0.863	4.394	4.509	-0.748	0.736	0.823
		$4X^{PC'}$	0.826	3.905	4.629	-0.770	0.920	1.290
		$4X^{PL'}$	0.804	4.012	5.004	-0.708	1.126	1.602

3. Various possible geometries and relative energies of SAA and PSA

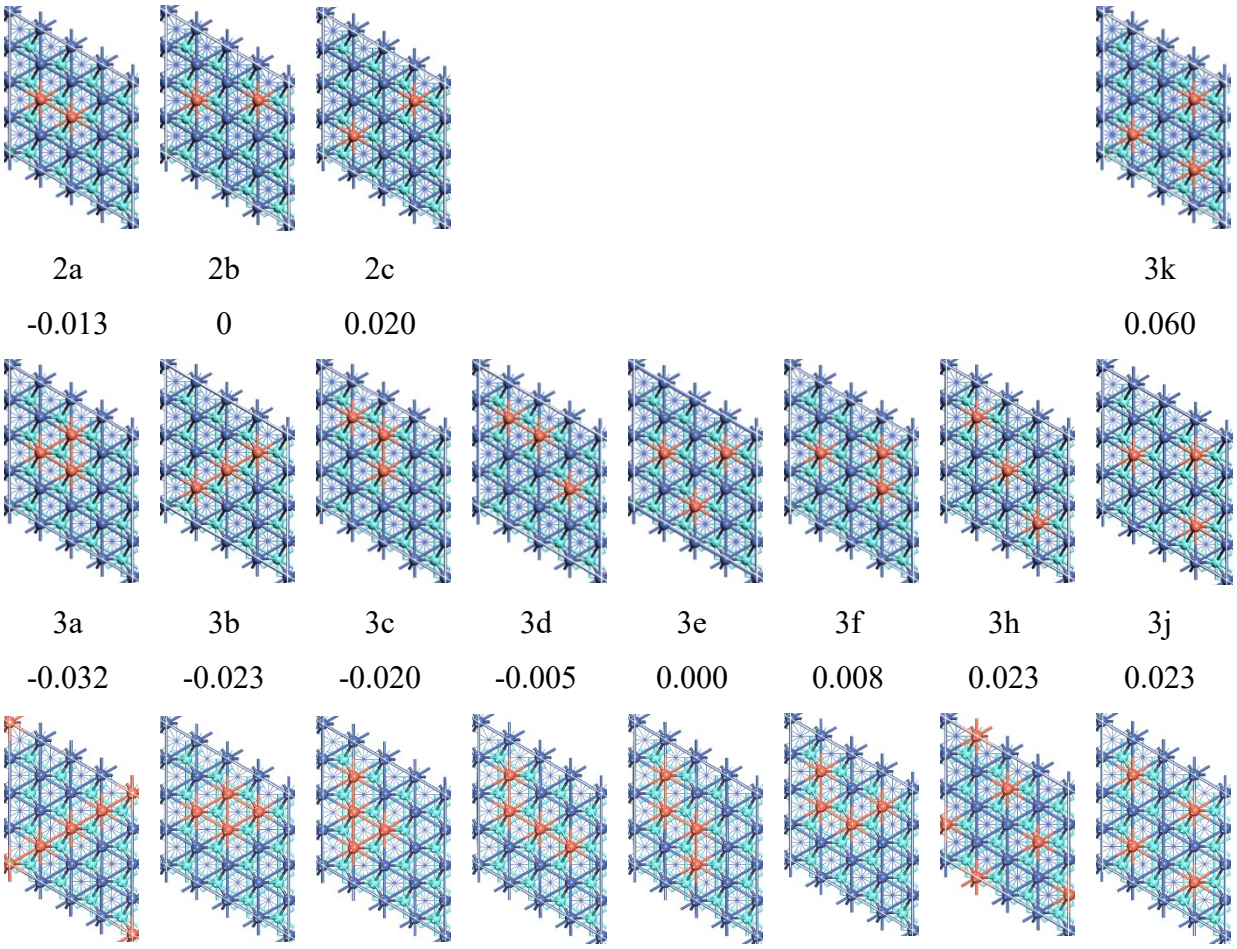

Figure S1. Various geometries and relative energies (in eV) of nCu/Ni(111) (n = 2 ~ 4)

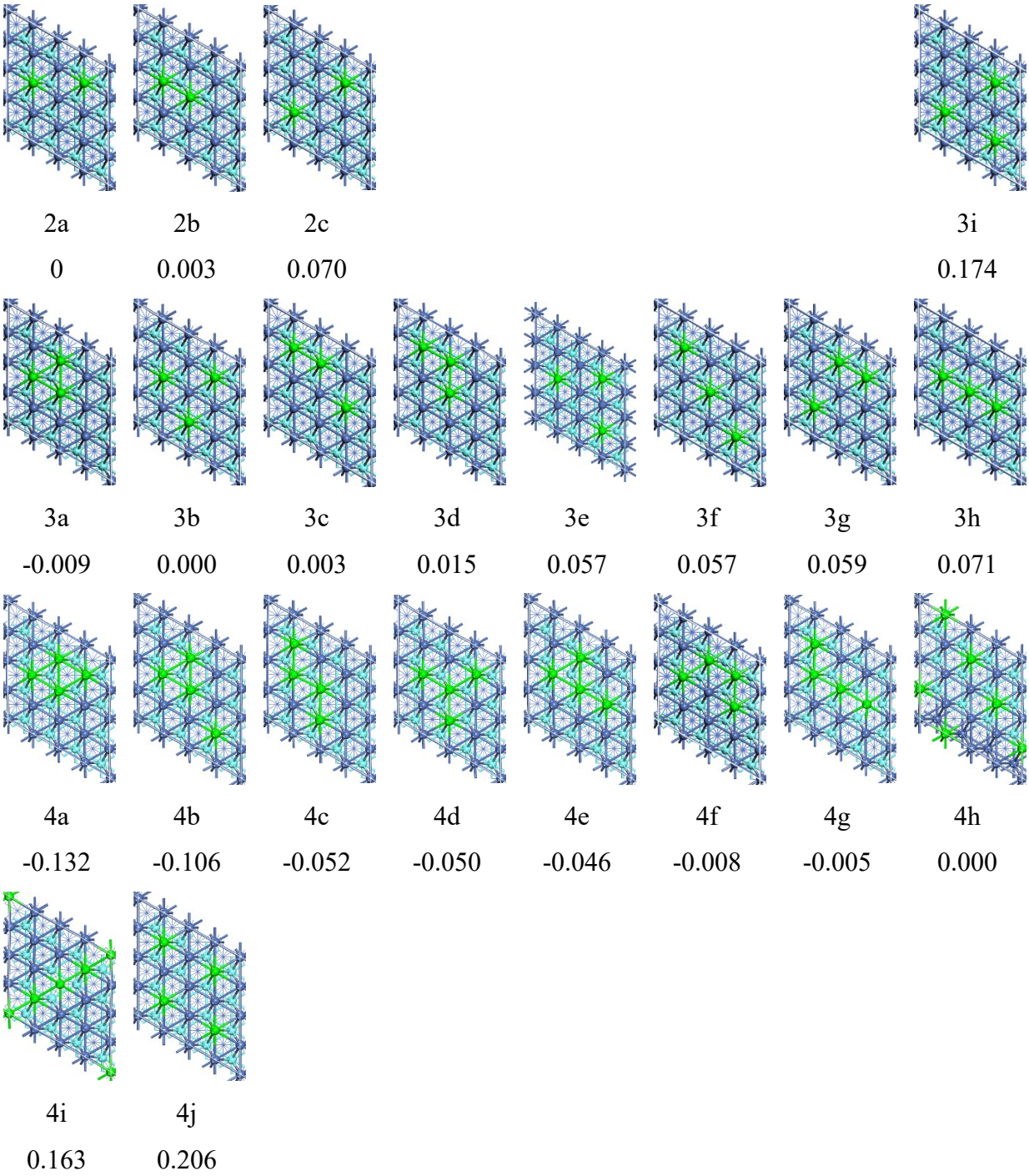

Figure S2. Various geometries and relative energies (in eV) of nAg/Ni(111) (n = 2 ~ 4).

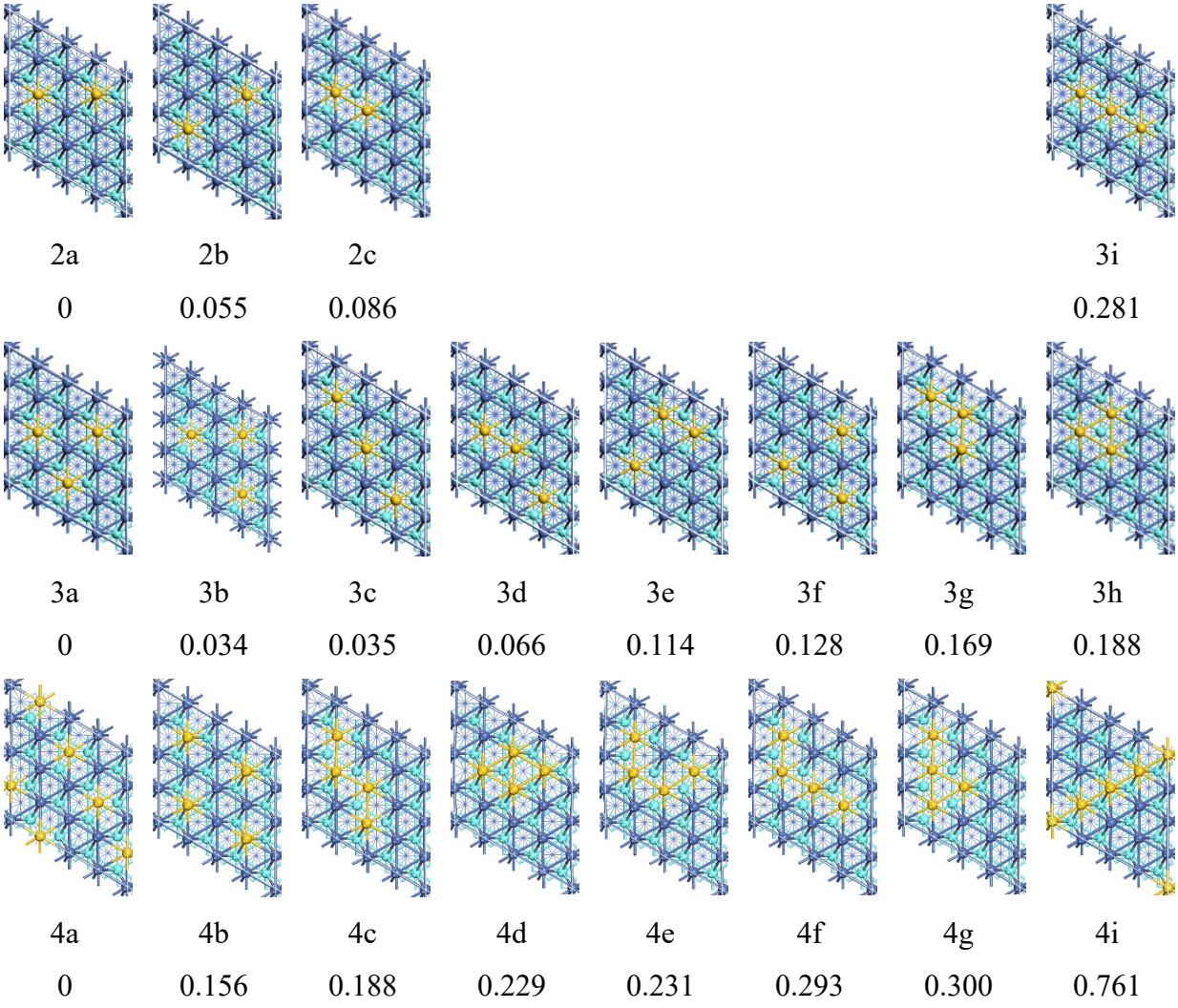

Figure S3. Various geometries and relative energies (in eV) of nAu/Ni(111) (n = 2 ~ 4).

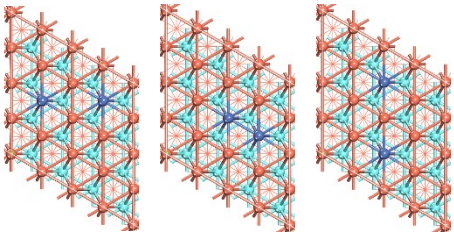

2a 2b 2c

0 0.006 0.008

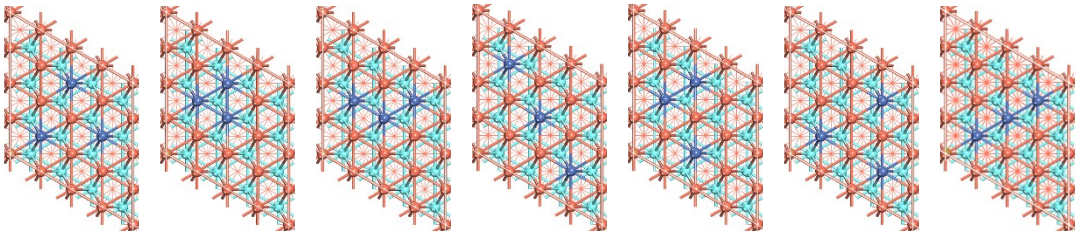

3a 3b 3c 3d 3e 3f 3g

0 0.003 0.005 0.006 0.011 0.021 0.023

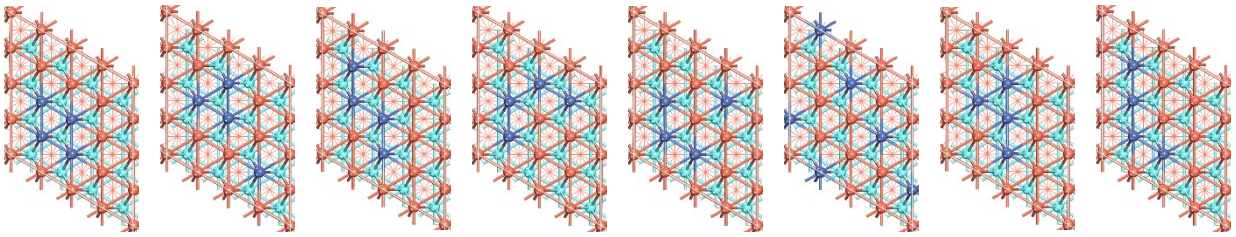

4a 4b 4c 4d 4e 4f 4g 4h

-0.022 -0.015 -0.011 -0.002 -0.002 0.000 0.001 0.006

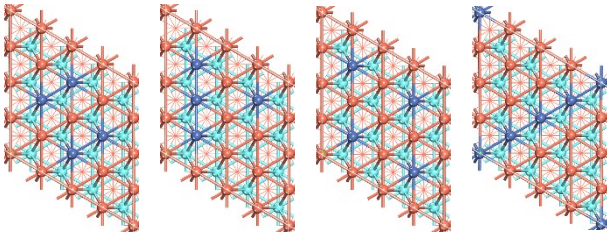

4i 4j 4k 4l

0.006 0.020 0.028 0.046

Figure S4. Various geometries and relative energies (in eV) of nNi/Cu(111) (n = 2 ~ 4).

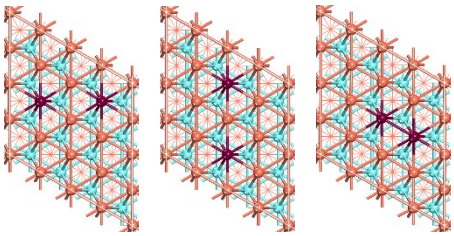

2a 2b 2c

0 0.019 0.084

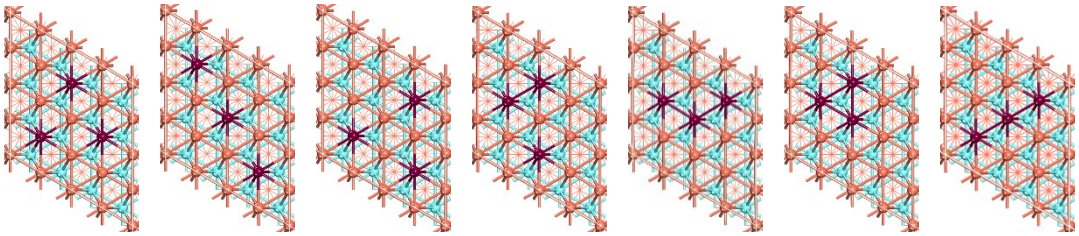

3a 3b 3c 3d 3e 3f 3g

0 0.016 0.051 0.100 0.175 0.213 0.229

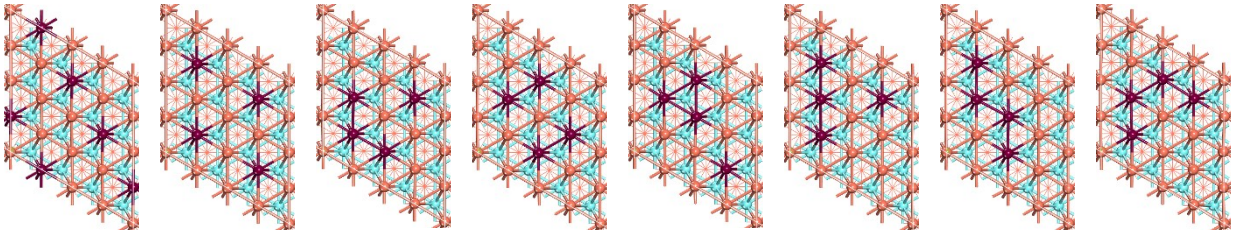

4a 4b 4c 4d 4e 4f 4g 4h

0 0.061 0.160 0.168 0.184 0.223 0.239 0.252

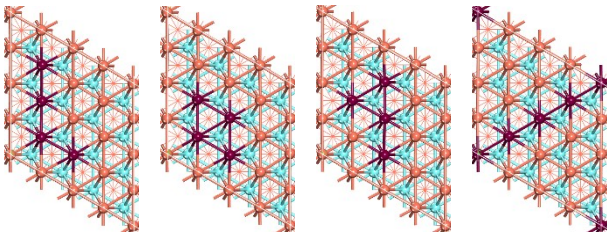

4i 4j 4k 4k

0.283 0.328 0.329 0.517

Figure S5. Various geometries and relative energies (in eV) of nPd/Cu(111) (n = 2 ~ 4)

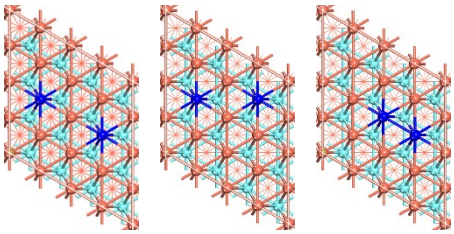

2a	2b	2c
0	0.007	0.123

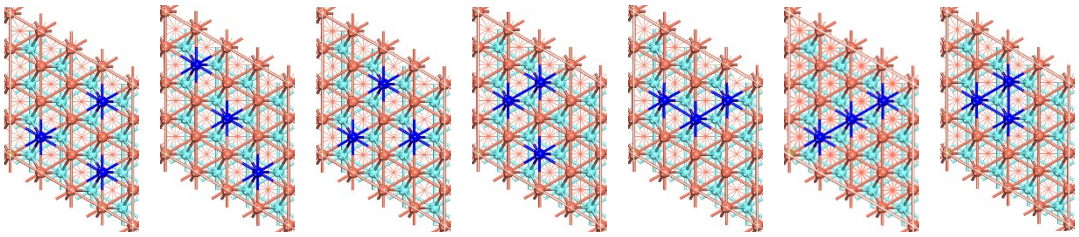

3a	3b	3c	3d	3e	3f	3g
0	0.015	0.028	0.131	0.255	0.304	0.314

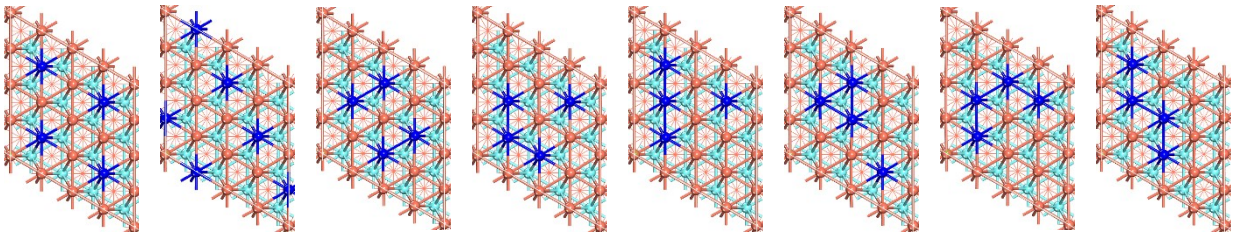

4a	4b	4c	4d	4e	4f	4g	4h
0	0.038	0.264	0.277	0.308	0.364	0.387	0.407

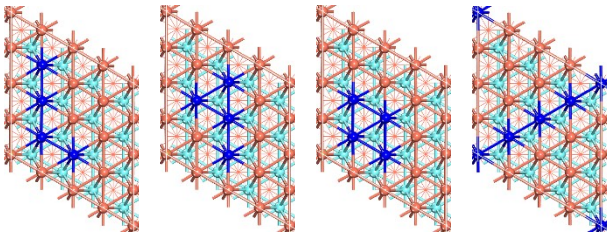

4i	4j	4k	4l
0.443	0.499	0.523	0.752

Figure S6. Various geometries and relative energies (in eV) of nPt/Cu(111) (n = 2 ~ 4)

4. The geometries of the SAA and PSA explored in this work

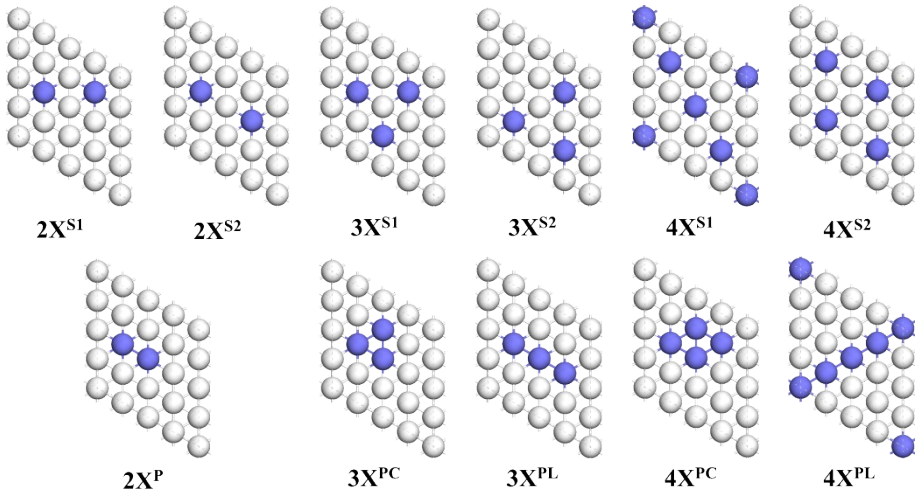

Scheme S2. Illustration of the SAA and PSA geometries

5. geometries employed in discussion on the energy changes in formations of SAA and PSA from M(111) and nX atoms

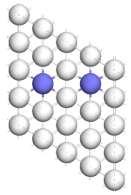

2X^{S1}

2X/Ni(111), X = Cu, Ag, Au

2X/Cu(111), X = Ni, Pd

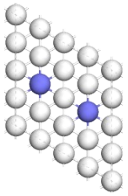

2X^{S2}

2X/Cu(111), X = Pt

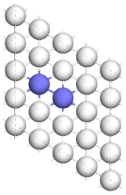

2X^{P}

2X/Ni(111), X = Cu, Ag, Au

2X/Cu(111), X = Ni, Pd, Pt

The geometries employed in Table 2

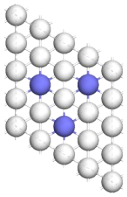

3X^{S1}

3X/Ni(111), X = Cu, Ag, Au

3X/Cu(111), X = Ni, Pd

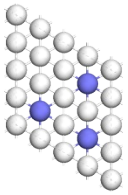

3X^{S2}

3X/Cu(111), X = Pt

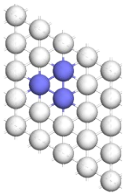

3X^{PC}

3X/Ni(111), X = Cu, Ag, Au

3X/Cu(111), X = Ni, Pd, Pt

The geometries employed in Table S5

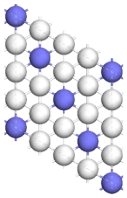

4X^{S1}

4X/Ni(111), X = Cu, Ag, Au

4X/Cu(111), X = Ni, Pd

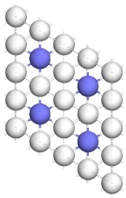

4X^{S2}

4X/Cu(111), X = Pt

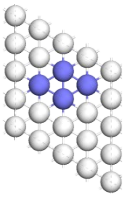

4X^{PC}

4X/Ni(111), X = Cu, Ag, Au

4X/Cu(111), X = Ni, Pd, Pt

The geometries employed in Table S6

Scheme S3. Geometries of nX/M(111) employed in Tables 2, 3, S4, and S5.

6. Energy changes in SAA formation and PSA formation from M(111) and nX atoms

Table S4. The assumed procedure to form the SAA and PSA structures of 3X/M(111)[a] from M(111) + 3X

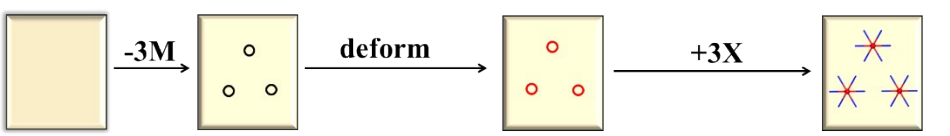

		E_{rm}^{3S} b)	E_{def}^{3S} b)	E_{int}^{3S} b)	ΔE_{tot}^{3S}
	Cu	17.600 eV	0.089 eV	-14.034 eV	3.655 eV
Ni(111)	Ag	17.600	0.086	-10.594	7.092
	Au	17.600	0.195	-13.674	4.121
	Ni	12.391	0.078	-16.237	-3.768
Cu(111)	Pd	12.391	0.111	-15.129	-2.627
	Pt	12.185 c)	0.315	-20.792	-8.292

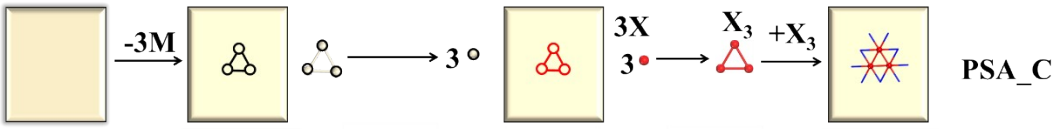

		E_{rm}^{3P} d)	$E_{dis,M3}^{3P}$ d)	E_{def}^{3P} d)	$E_{f,X3}^{3P}$ d)	E_{int}^{3P} d)	ΔE_{tot}^{3P}
	Cu	11.638 eV	4.949 eV	0.139 eV	-3.399 eV	-9.732 eV	3.594 eV
Ni(111)	Ag	11.638	4.949	0.180	-2.532	-7.151	7.083
	Au	11.638	4.949	0.248	-3.466	-9.088	4.280
	Ni	8.199	3.361	0.141	-4.885	-10.581	-3.765
Cu(111)	Pd	8.199	3.361	0.115	-3.360	-10.729	-2.414
	Pt	8.199	3.361	0.211	-6.617	-13.132	-7.978

a) The SAA_S2 structure of 3Pt/Cu(111)^S and the SAA_S1 structure of the other 3X/M(111)^S are used in the SAA part and the PSA_C is used in all 3X/M(111)^P cases here. b) E_{rm}^{3S}, E_{def}^{3S}, and E_{int}^{3S} are defined by eqs (1), (2), and (3). c) This value differs from E_{rm}^{3S} of 3Ni/Cu(111) and 3Pd/Cu(111) because 3Pt/Cu(111) has the S2 structure in which two Pt atoms are separated by one Cu atom but 3Ni/Cu(111) and 3Pd/Cu(111) have the S1 structure in which two X atoms (X = Ni or Pd) are separated by one Cu-Cu bond and other two X atoms are separated by one Cu atom, as shown in Table 1, Scheme 1, and Scheme S3 of the SI. d) E_{rm}^{3P}, $E_{dis,M3}^{3P}$, $E_{f,X3}^{3P}$, and E_{int}^{3P} are defined by eqs (5), (6), (7), (8) and (9). All these terms are given in eV unit.

In Table S4, the ΔE_{tot} becomes more positive in the order PSA_C < SAA in 3Cu/Ni(111) and 3Ag/Ni(111), and in the order SAA < PSA_C in 3Au/Ni(111), 3Ni/Cu(111), 3Pd/Cu(111), and 3Pt/Cu(111). These results are in agreement with the relative stabilities, as shown in Table 1.

When going from 3Cu/Ni(111) to 3Au/Ni(111), the E_{def}^{3S} term gets more positive by 0.106 eV in the SAA, while the E_{def}^{3P} term increases by 0.109 eV in the PSA_C; The E_{int}^{3S} gets less negative by 0.360 eV, while the $E_{f,X3}^{3P} + E_{int}^{3P}$ gets less negative by 0.577 eV. The change in the difference between the E_{def}^{3S} and E_{def}^{3P} is -0.003 eV, which is much smaller than that of -0.217 eV between the E_{int}^{3S} and the $E_{f,X3}^{3P} + E_{int}^{3P}$. These results indicate that the important factor in determining the formation of 3Cu/Ni(111)^{P} and 3Au/Ni(111)^{S} is the much less decrease in the E_{int}^{3S} than in the $E_{f,X3}^{3P} + E_{int}^{3P}$ when going from X = Cu to X = Au.

When going from 3Cu/Ni(111) to 3Ag/Ni(111), the E_{def}^{3S} term gets less positive by 0.003 eV in the SAA, while the E_{def}^{3P} term gets more positive by 0.041 eV in the PSA_C. The E_{int}^{3S} gets less negative by 3.440 eV in the SAA, while the $E_{f,X3}^{3P} + E_{int}^{3P}$ increases gets less negative by 3.348 eV in the PSA_C. These results show that the important factor in determining the formation of 3Cu/Ni(111)^{P} and 3Ag/Ni(111)^{P} is the much more decrease in the E_{int}^{3S} than in the $E_{f,Xn}^{nP} + E_{int}^{nP}$ when going from X = Cu to X = Ag.

In 3X/Cu(111), when going from X = Ni to X = Pd, the E_{def}^{3S} gets more positive by 0.033 eV in the SAA, while the E_{def}^{3P} gets less positive by 0.026 eV in the PSA_C. The E_{int}^{3S} gets less negative by 1.108 eV in the SAA. The $E_{int}^{3P} + E_{f,X3}^{3P}$ gets less negative by 1.377 eV in the PSA_C, whose decrease is larger than that of the E_{int}^{3S} term by 0.269 eV. Because of the larger decrease in the $E_{int}^{3P} + E_{f,X3}^{3P}$ than in the E_{int}^{3S}, the SAA becomes more stable than the PSA in 3Pd/Cu(111).

When going from X = Ni to X = Pt, the E_{rm}^{3S} gets more positive by 0.026 eV in the SAA, while the E_{rm}^{3P} term does not change in the PSA_C. The E_{def}^{3S} gets more positive by 0.237 eV in the

SAA. The E_{def}^{3P} gets more positive by 0.070 eV in the PSA_C, whose increase is smaller than the E_{int}^{3S} gets more negative by 0.167 eV. The E_{int}^{3S} gets more negative by 4.555 eV in the SAA. The $E_{int}^{3P} + E_{f,X3}^{3P}$ gets more negative by 4.283 eV in the PSA_C, whose increase is much smaller than that of the E_{int}^{3S} term by 0.272 eV. Apparently, the change in the stabilization energy is larger than that in the destabilization energy. Because of the larger decrease in the $E_{int}^{3P} + E_{f,Xn}^{3P}$ than in the E_{int}^{3S}, the SAA becomes more stable than the PSA in 3Pt/Cu(111).

Table S5. The assumed procedure to form the SAA and PSA structures of 4X/M(111)[a] from M(111) + 4X

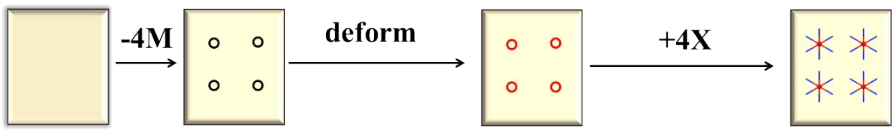

		E_{rm}^{4S} b)	E_{def}^{4S} b)	E_{int}^{4S} b)	ΔE_{tot}^{4S}
	Cu	23.454 eV	0.305 eV	-18.847 eV	4.912 eV
Ni(111)	Ag	23.454	0.264	-14.093	9.652
	Au	23.454	0.434	-18.202	5.686
	Ni	16.606	0.108	-21.534	-4.820
Cu(111)	Pd	16.606	0.179	-20.039	-3.254
	Pt	16.268 c)	0.380	-27.502	-10.854

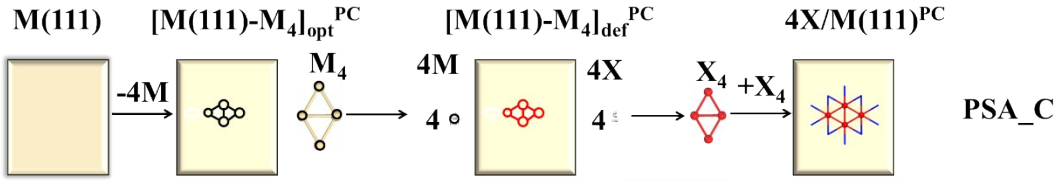

		E_{rm}^{4P} d)	$E_{dis,M4}^{4P}$ d)	E_{def}^{4P} d)	$E_{f,X4}^{4P}$ d)	E_{int}^{4P} d)	ΔE_{tot}^{4P}
	Cu	13.986 eV	7.845 eV	0.162 eV	-5.942 eV	-11.248 eV	4.804 eV
Ni(111)	Ag	13.986	7.845	0.215	-4.428	-8.125	9.494
	Au	13.986	7.845	0.287	-6.036	-10.167	5.916
	Ni	9.469	5.886	0.167	-7.809	-12.554	-4.841
Cu(111)	Pd	9.469	5.886	0.142	-5.637	-12.787	-2.927
	Pt	9.469	5.886	0.256	-10.101	-15.841	-10.331

a) The most stable structure presented in Table 1 is employed here. b) E_{rm}^{4S}, E_{def}^{4S}, and E_{int}^{4S} are defined by eqs. (1), (2), and (3). c) This value differs from E_{rm}^{4S} of 4Ni/Cu(111) and 4Pd/Cu(111) because 4Pt/Cu(111) has the S2 structure in which two Pt atoms are separated by one Cu atom but 4Ni/Cu(111) and 4Pd/Cu(111) have the S1 structure in which two X atoms (X = Ni or Pd) are separated by one Cu-Cu bond and other two X atoms are separated by one Cu atom, as shown in Table 1, Scheme 1, and Scheme S3 of the SI. d) E_{rm}^{4P}, $E_{dis,M4}^{4P}$, $E_{f,X4}^{4P}$, and E_{int}^{4P} are defined by eqs. (5), (6), (7), (8) and (9). All these terms are in eV unit.

In Table S5, the ΔE_{tot} becomes more positive in the order PSA_C < SAA in 4Cu/Ni(111), 4Ag/Ni(111), and 4Ni/Cu(111), and in the order SAA < PSA_C in 4Au/Ni(111), 4Pd/Cu(111), and 4Pt/Cu(111). These trends agree with the relative stabilities, shown in Table 1.

When going from 4Cu/Ni(111) to 4Au/Ni(111), the E_{def}^{4S} term gets more positive by 0.129 eV in the SAA, while the E_{def}^{4P} term gets more positive by 0.125 eV in the PSA_C; The E_{int}^{4S} gets less negative by 0.645 eV in the SAA, while the $E_{f,X4}^{4P} + E_{int}^{4P}$ gets less negative by 0.987 eV in the PSA_C. These results show that the important factor to afford 4Cu/Ni(111)^{P} and 4Au/Ni(111)^{S} is the much less decrease in the E_{int}^{4S} than in the $E_{f,X4}^{4P} + E_{int}^{4P}$ when going from 4Cu/Ni(111) to 4Au/Ni(111).

When going from 4Cu/Ni(111) to 4Ag/Ni(111), the E_{def}^{4S} term gets less positive by 0.041 eV in the SAA, while the E_{def}^{4P} term gets more positive by 0.053 eV in the PSA_C; The E_{int}^{4S} gets less negative by 4.754 eV in the SAA, while the $E_{f,X4}^{4P} + E_{int}^{4P}$ gets less negative by 4.637 eV in the PSA_C. These results show that the important factor to help the formation of 4Cu/Ni(111)^{P} and 4Ag/Ni(111)^{P} is the much more decrease in the E_{int}^{4S} than in the $E_{f,X4}^{4P} + E_{int}^{4P}$ when going from 4Cu/Ni(111) to 4Ag/Ni(111).

When going from 4Ni/Cu(111) to 4Pd/Cu(111), the E_{def}^{4S} term gets more positive by 0.071 eV in the SAA, and the E_{def}^{4P} term gets less positive by 0.025 eV in the PSA_C. The E_{int}^{4S} gets less negative by 1.495 eV in the SAA, while the $E_{f,X4}^{4P} + E_{int}^{4P}$ gets less negative by 1.939 eV in the PSA_C. These results indicate that the important factor to afford 4Ni/Cu(111)^{P} and 4Pd/Cu(111)^{S} is the much less decrease in the E_{int}^{4S} than in the $E_{f,X4}^{4P} + E_{int}^{4P}$ when going from 4Ni/Cu(111) to 4Pd/Cu(111).

When going from 4Ni/Cu(111) to 4Pt/Cu(111), the E_{rm}^{4S} gets less positive by 0.338 eV in the SAA and the $E_{rm}^{4P} + E_{dis,M4}^{4P}$ is the same in the PSA_C. The E_{def}^{4S} term gets more positive by 0.272 eV in the SAA, while the E_{def}^{4P} term gets less positive by 0.089 eV in the PSA_C; The E_{int}^{4S} gets more negative by 5.968 eV in the SAA, while the $E_{f,X4}^{4P} + E_{int}^{4P}$ gets more negative by 5.579

eV in the PSA_C. These results indicate that the important factor to afford 4Pt/Cu(111)^{S} is the larger increase in the E_{int}^{4S} than in the $E_{f,X4}^{4P} + E_{int}^{4P}$ when going from 4Ni/Cu(111) to 4Pt/Cu(111).

All the above results show that the E_{int} plays an important role in determining the relative stabilities of the SAA and PSA.

7. The Bader charge of nX atoms and X_n cluster, the Fermi level, *d* band center of nX/M(111)

Table S6. The Bader charge of each X atom in nX/M(111)

Alloys	nX/Ni(111)			nX/Cu(111)		
	X = Cu	X = Ag	X = Au	X = Ni	X = Pd	X = Pt
$2X^S$	0.02	-0.10	-0.45	-0.10	-0.37	-0.64
	0.02	-0.10	-0.45	-0.10	-0.37	-0.64
$2X^P$	0.00	-0.09	-0.39	-0.09	-0.33	-0.57
	0.01	-0.09	-0.38	-0.10	-0.33	-0.57
$3X^S$	0.01	-0.09	-0.43	-0.10	-0.36	-0.65
	0.01	-0.08	-0.43	-0.10	-0.36	-0.64
	0.01	-0.09	-0.43	-0.09	-0.36	-0.64
$3X^{PC}$	0.02	-0.01	-0.30	-0.08	-0.32	-0.52
	-0.01	-0.10	-0.34	-0.08	-0.31	-0.50
	0.00	-0.07	-0.34	-0.01	-0.29	-0.47
$4X^S$	0.02	-0.08	-0.42	-0.10	-0.36	-0.64
	0.02	-0.08	-0.42	-0.10	-0.36	-0.64
	0.02	-0.08	-0.42	-0.10	-0.36	-0.64
	0.02	-0.08	-0.43	-0.10	-0.36	-0.64
$4X^{PC}$	0.01	-0.08	-0.27	-0.09	-0.26	-0.45
	0.02	-0.08	-0.33	-0.09	-0.31	-0.48
	0.00	-0.08	-0.33	-0.09	-0.29	-0.50
	-0.01	-0.06	-0.27	-0.06	-0.29	-0.46

Table S7. The Bader charge of nX (Q in e) and the Fermi level (ε_F in eV) in nX/M(111)

Alloys		X	$2X^S$	$2X^P$	$3X^S$	$3X^{PC}$	$4X^S$	$4X^{PC}$
nCu/Ni(111)	Q	0.01	0.04	0.01	0.04	0.01	0.08	0.02
	ε_F	-5.06	-5.06	-5.06	-5.06	-5.06	-5.05	-5.05
nAg/Ni(111)	Q	-0.10	-0.20	-0.18	-0.26	-0.18	-0.32	-0.29
	ε_F	-5.06	-5.06	-5.06	-5.05	-5.04	-5.04	-5.04
nAu/Ni(111)	Q	-0.46	-0.90	-0.77	-1.29	-0.98	-1.68	-1.19
	ε_F	-5.09	-5.13	-5.13	-5.17	-5.15	-5.20	-5.17
nNi/Cu(111)	Q	-0.09	-0.19	-0.18	-0.29	-0.17	-0.42	-0.33
	ε_F	-4.77	-4.77	-4.77	-4.77	-4.78	-4.79	-4.81
nPd/Cu(111)	Q	-0.39	-0.73	-0.66	-1.08	-0.92	-1.45	-1.16
	ε_F	-4.77	-4.78	-4.78	-4.78	-4.79	-4.81	-4.82
nPt/Cu(111)	Q	-0.65	-1.29	-1.14	-1.92	-1.50	-2.62	-1.89
	ε_F	-4.80	-4.84	-4.84	-4.88	-4.89	-4.94	-4.96

Table S8. The *d* band center ($\varepsilon_{dc\text{-}tot}$) and *d* band center in the valence level ($\varepsilon_{dc\text{-}VB}$) of the first-layer atoms on nAg/Ni(111) and nPd/Cu(111) alloys.

nX^1/Ni(111)	$\varepsilon_{dc\text{-}tot}$	$\varepsilon_{dc\text{-}VB}$	nX^2/Cu(111)	$\varepsilon_{dc\text{-}tot}$	$\varepsilon_{dc\text{-}VB}$
nX^1	nCu/Ni(111)^S		nX^2	nNi/Cu(111)^S	
$2Cu^{S1}$	-4.83	-6.84	$2Ni^{S1}$	-5.85	-7.13
$3Cu^{S1}$	-4.89	-6.87	$3Ni^{S1}$	-5.67	-7.00
$4Cu^{S1}$	-4.96	-6.88	$4Ni^{S1}$	-5.55	-6.89
	nAg/Ni(111)^S			nPd/Cu(111)^P	
$2Ag^{S1}$	-4.99	-7.08	$2Pd^P$	-5.94	-7.29
$3Ag^{S1}$	-5.13	-7.22	$3Pd^{PC}$	-5.83	-7.24
$4Ag^{S1}$	-5.24	-7.31	$4Pd^{PC}$	-5.74	-7.21
	nAu/Ni(111)^P			nPt/Cu(111)^P	
$2Au^P$	-5.05	-7.14	$2Pt^P$	-6.03	-7.38
$3Au^{PC}$	-5.21	-7.32	$3Pt^{PC}$	-5.98	-7.39
$4Au^{PC}$	-5.37	-7.49	$4Pt^{PC}$	-5.94	-7.43

8. PDOSs of M(111) and nX/M(111)

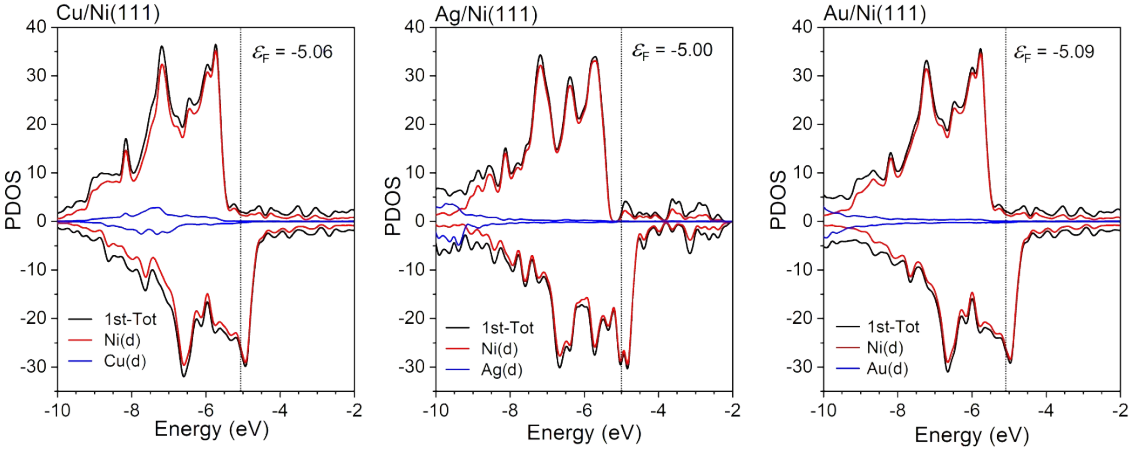

Figure S7. The PDOS of the top-layer in X/Ni(111) (X = Cu, Ag, Au)

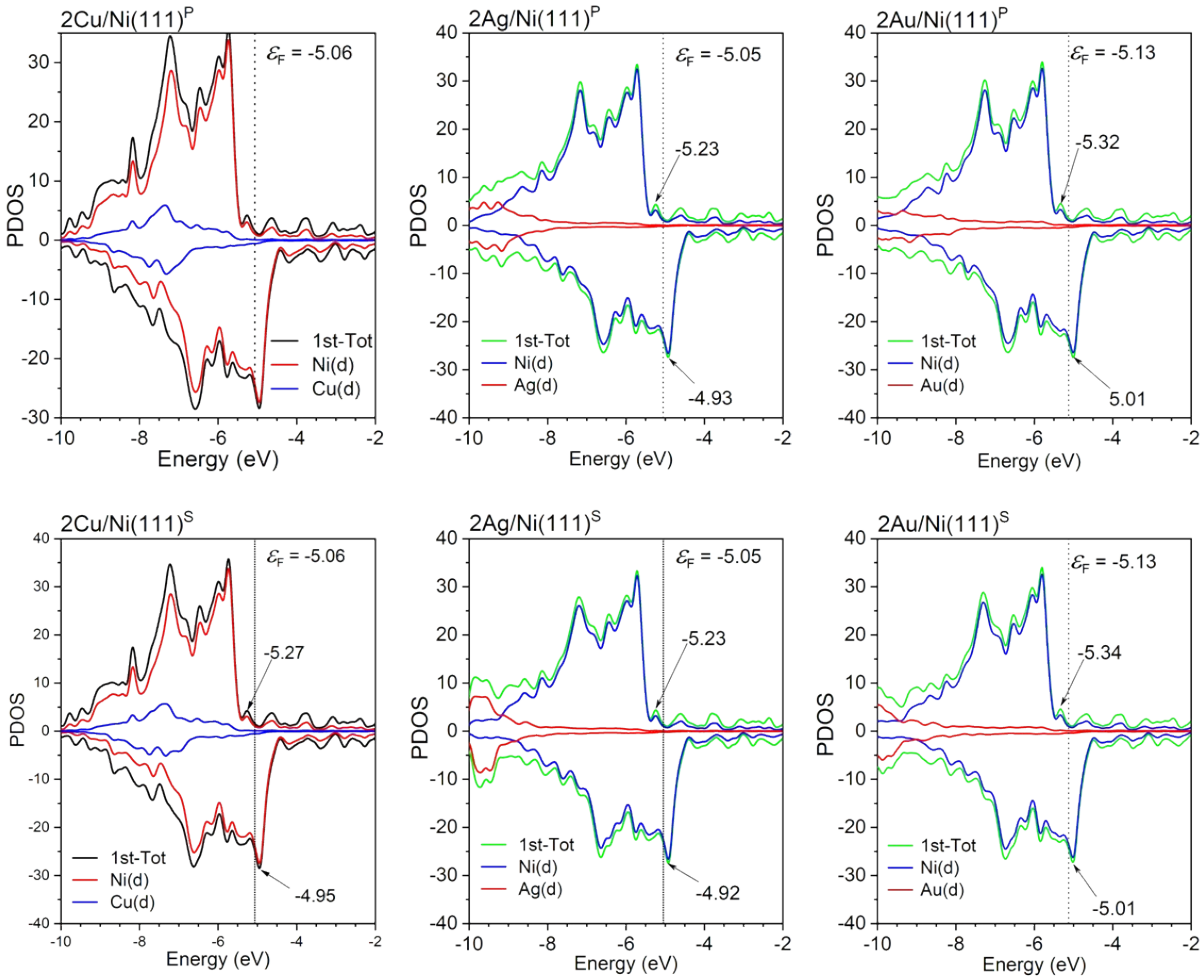

Figure S8. The PDOS of the top-layer in 2X/Ni(111) (X = Cu, Ag, Au)

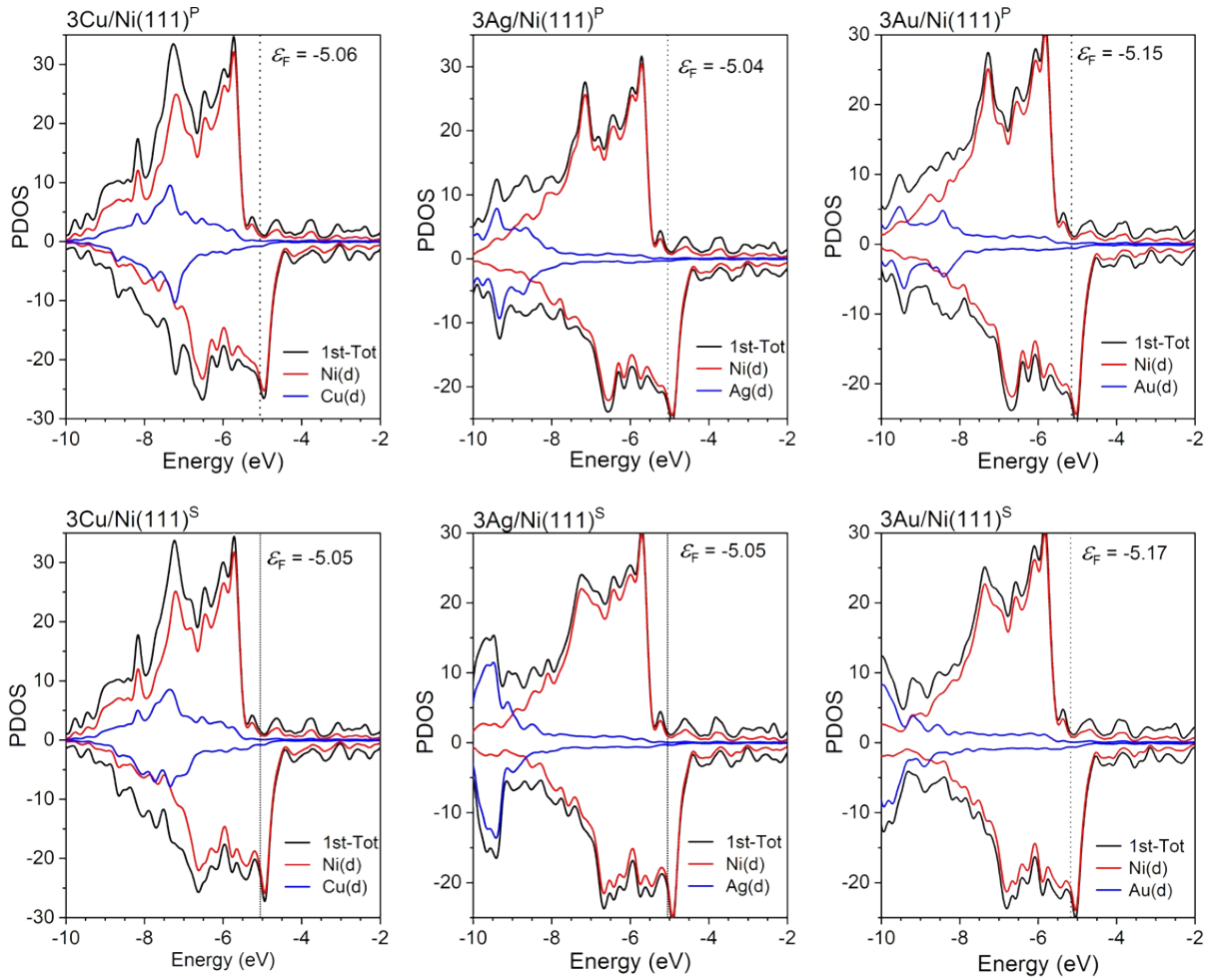

Figure S9. The PDOS of the top-layer in 3X/Ni(111) (X = Cu, Ag, Au)

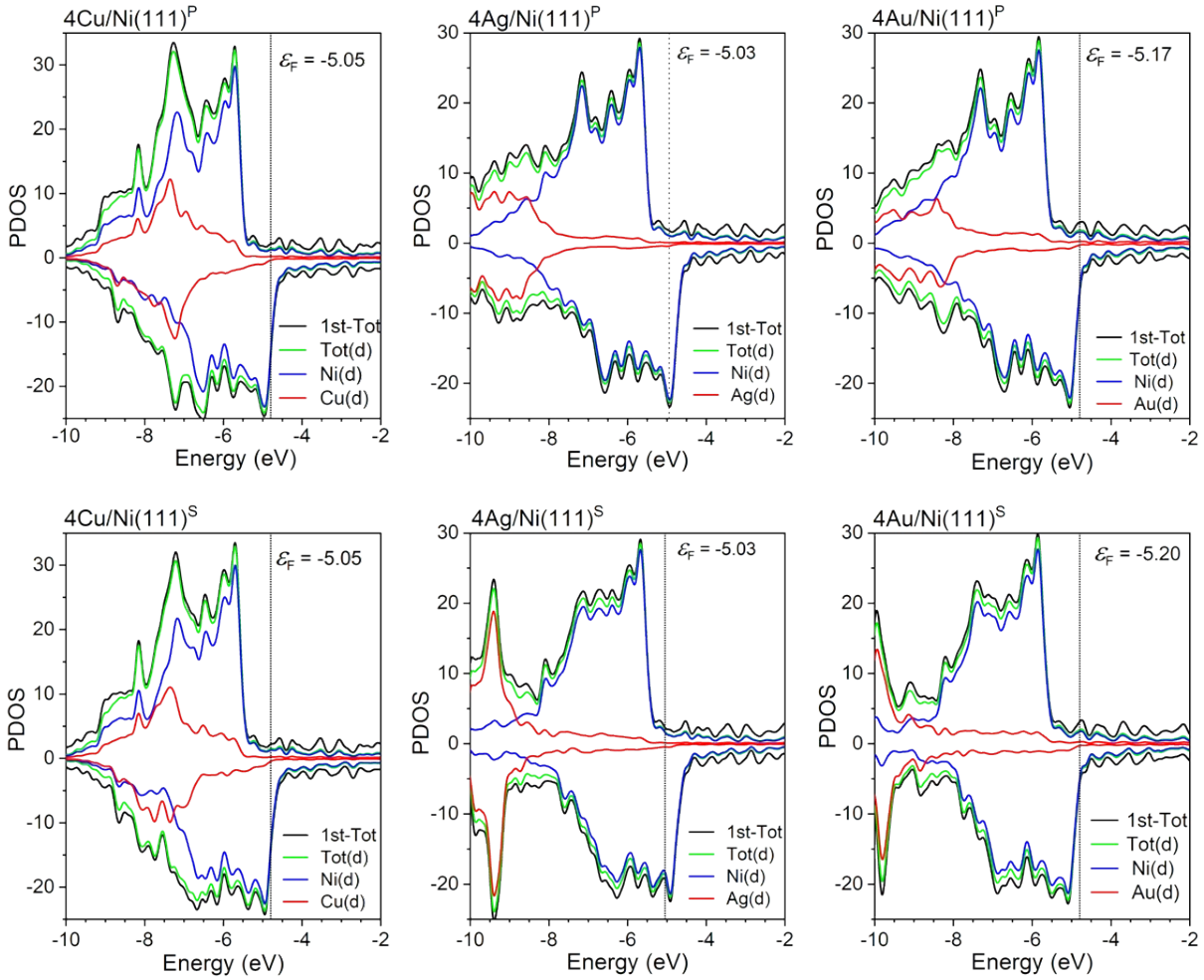

Figure S10. The PDOS of the top-layer in 4X/Ni(111) (X = Cu, Ag, Au)

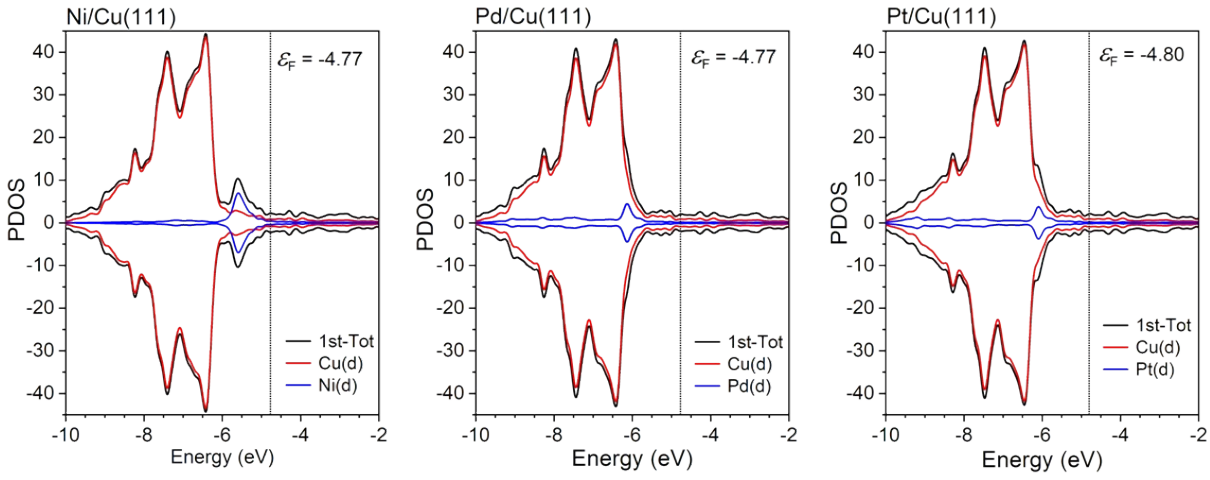

Figure S11. The PDOS of the top-layer in X/Cu(111) (X = Ni, Pd, Pt)

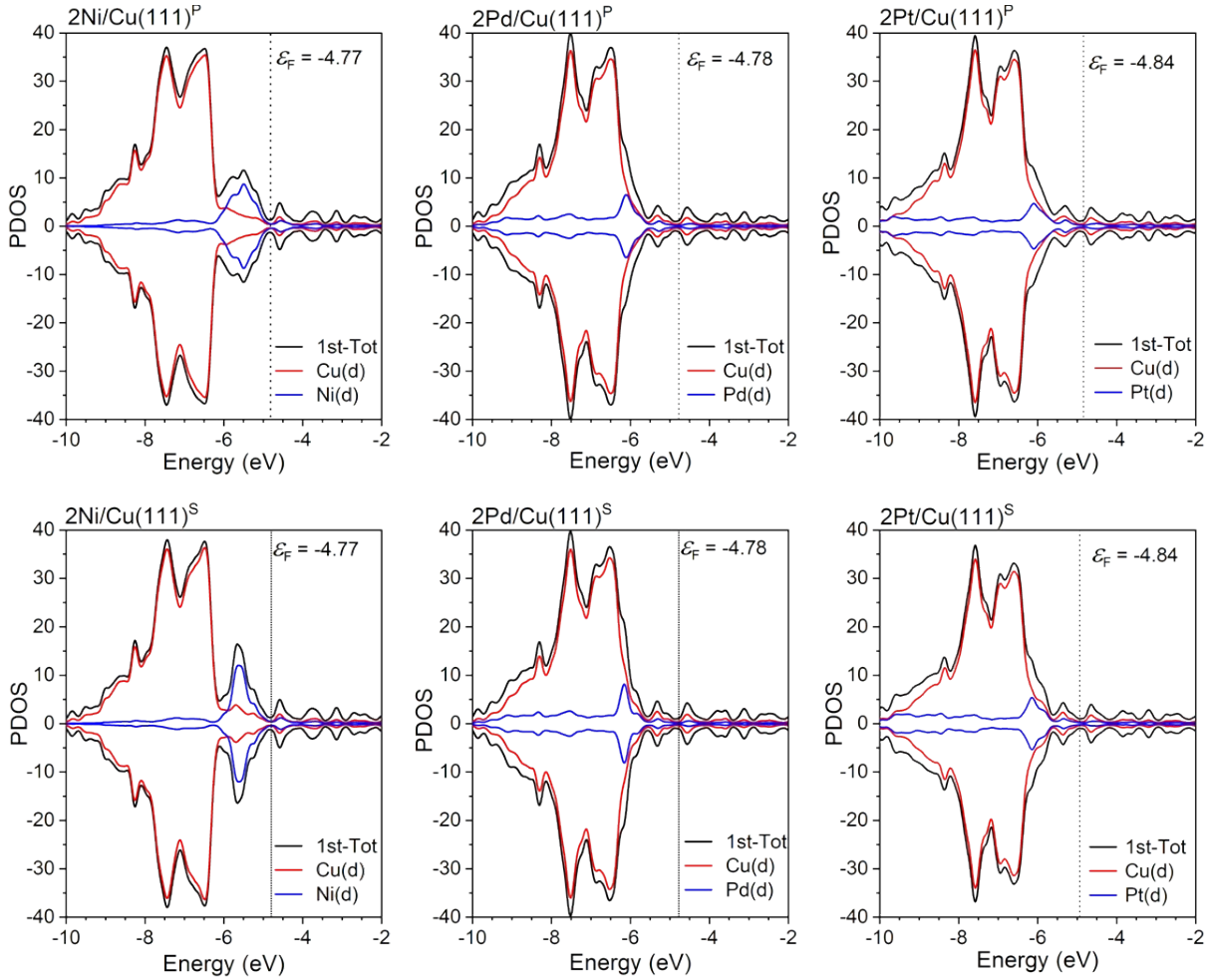

Figure S12. The PDOS of the top-layer in 2X/Cu(111) (X = Ni, Pd, Pt)

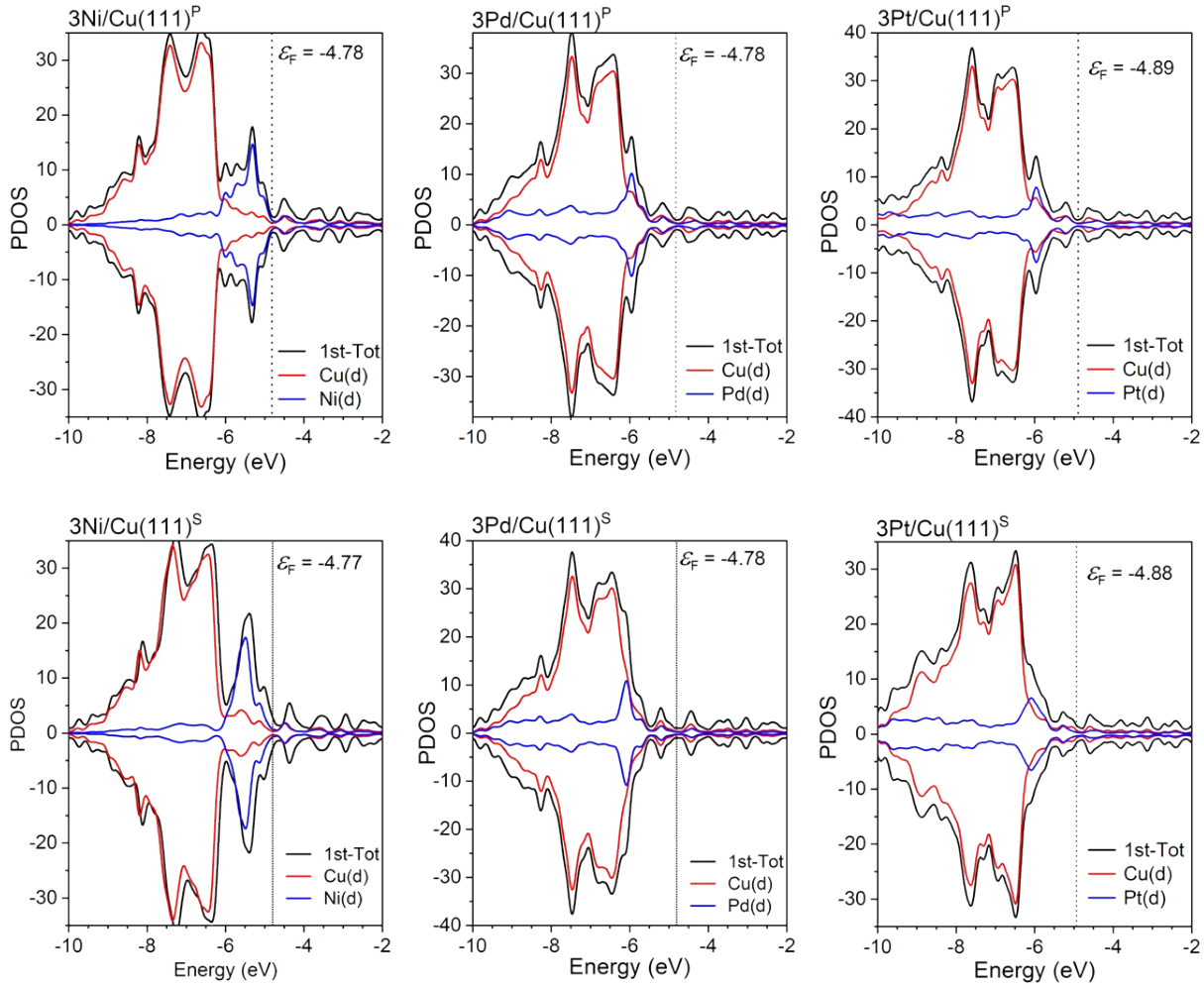

Figure S13. The PDOS of the top-layer in 3X/Cu(111) (X = Ni, Pd, Pt)

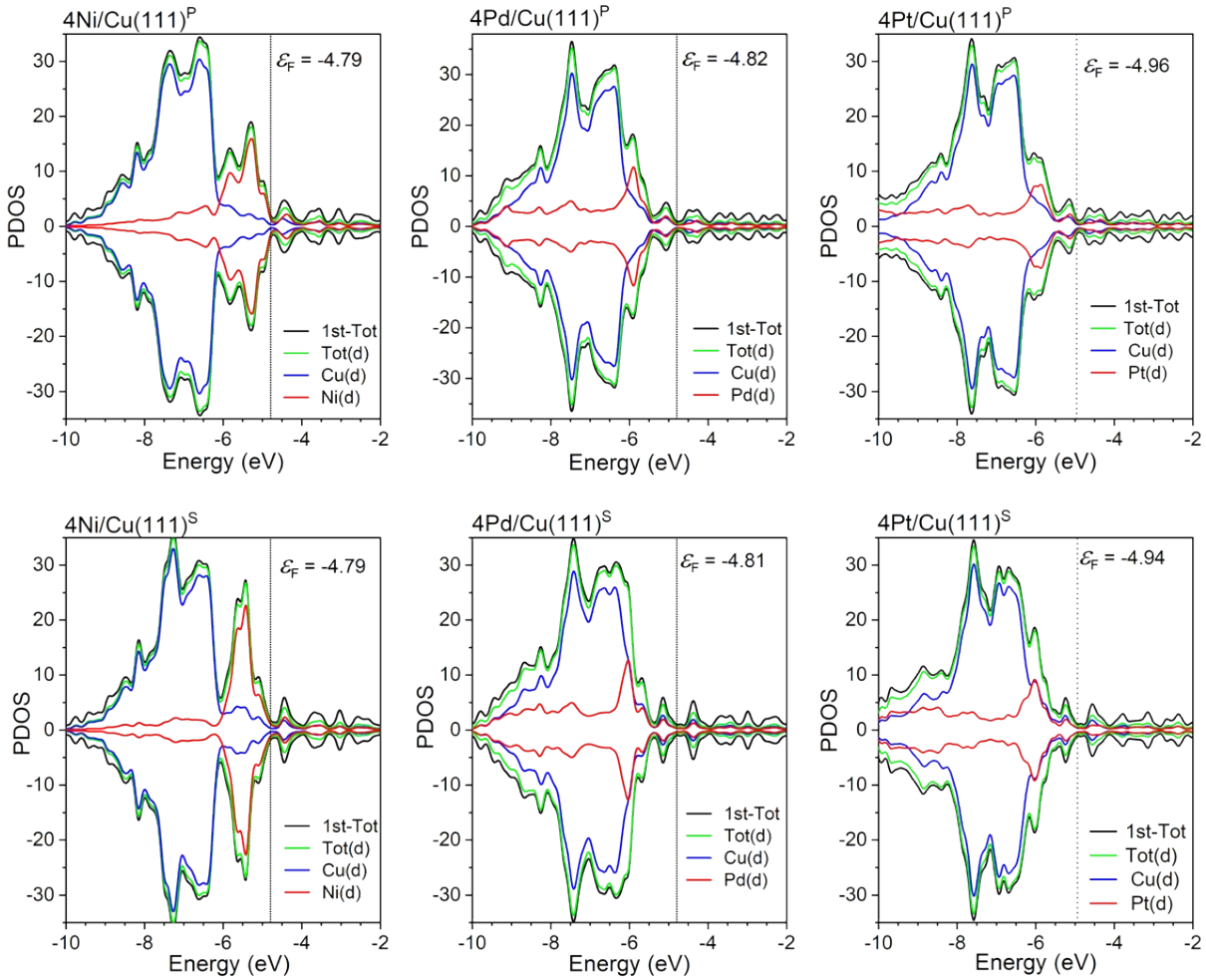

Figure S14. The PDOS of the top-layer in 4X/Cu(111) (X = Ni, Pd, Pt)

9. Spin density of M around X in nX/M(111)

Table S9. The averaged magnetic moments of the M atoms connected to the X atoms and those of the rest M atoms in nX/M(111).

nX/M(111)	Averaged magnetic moment on M [a)]			Averaged magnetic moment on M [b)]		
nX/Ni(111)	X=Cu	X = Ag	X = Au	X=Cu	X = Ag	X = Au
1X	0.665	0.652	0.667	0.678	0.658	0.679
$2X^S$	0.664	0.669	0.665	0.682	0.680	0.682
$3X^S$	0.659	0.651	0.661	0.681	0.683	0.680
$4X^S$	0.639	0.646	0.643	0.676	0.675	0.678
$2X^P$	0.658	0.663	0.661	0.683	0.682	0.682
$3X^P$	0.649	0.655	0.657	0.682	0.680	0.680
$4X^P$	0.636	0.645	0.652	0.676	0.676	0.679
nX/Cu(111)	X=Ni	X = Pd	X = Pt	X=Ni	X = Pd	X = Pt
1X	0.000	0.000	0.000	0.000	0.000	0.000
$2X^S$	0.000	0.000	0.000	0.000	0.000	0.000
$3X^S$	0.000	0.000	0.000	0.000	0.000	0.000
$4X^S$	0.000	0.000	0.000	0.000	0.000	0.000
$2X^P$	0.000	0.000	0.000	0.000	0.000	0.000
$3X^P$	0.000	0.000	0.000	0.000	0.000	0.000
$4X^P$	0.000	0.000	0.000	0.000	0.000	0.000

a): the averaged magnetic moment among the M atoms connected to the X atoms.

b): the averaged magnetic moment among the rest M moiety except those M atoms connected to the X atoms.

10. A-B bond strength and valence orbital energies of A and B

Stabilization energy ΔE(A-B) by spin pairing is approximately represented by the equation $\Delta E(A-B) = \sqrt{(\epsilon_A - \epsilon_B)^2 + 4\beta^2}$ on the basis of simple Hückel MO theory, where ϵ_A and ϵ_B are valence orbital energies of A and B, respectively, and β is resonance integral. This equation indicates that ΔE(A-B) becomes larger as the energy difference in valence orbital $(\epsilon_A - \epsilon_B)$ increases when β does not differ very much, as is shown in Scheme S4. The larger orbital energy difference between the X atom / X_n cluster and the [M(111) – nM] host with defects leads to the formation of stronger interaction with a larger stabilization energy.

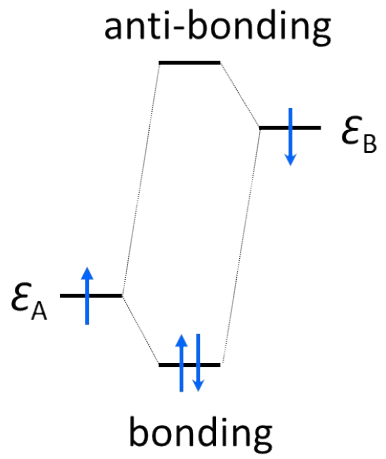

Scheme S4. Orbital interaction between A and B species

11. Frontier orbitals of X_n clusters in nX/M(111)^P

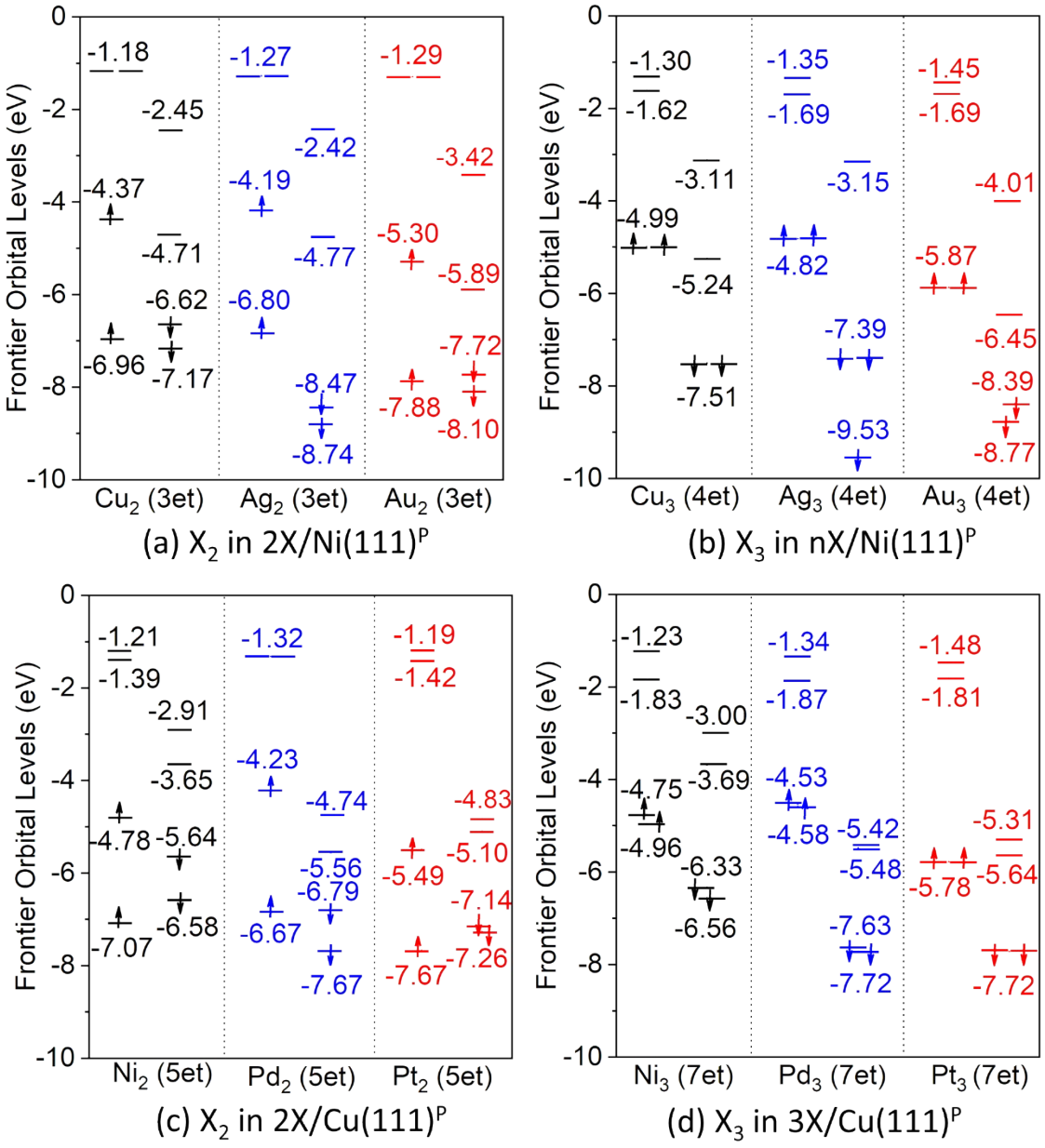

Figure S15. Energy levels of frontier orbitals of X_2 and X_3 clusters, where the geometry of X_n cluster was taken to be the same as that of nX/M(111)^P at the B3LYP/SDD level.

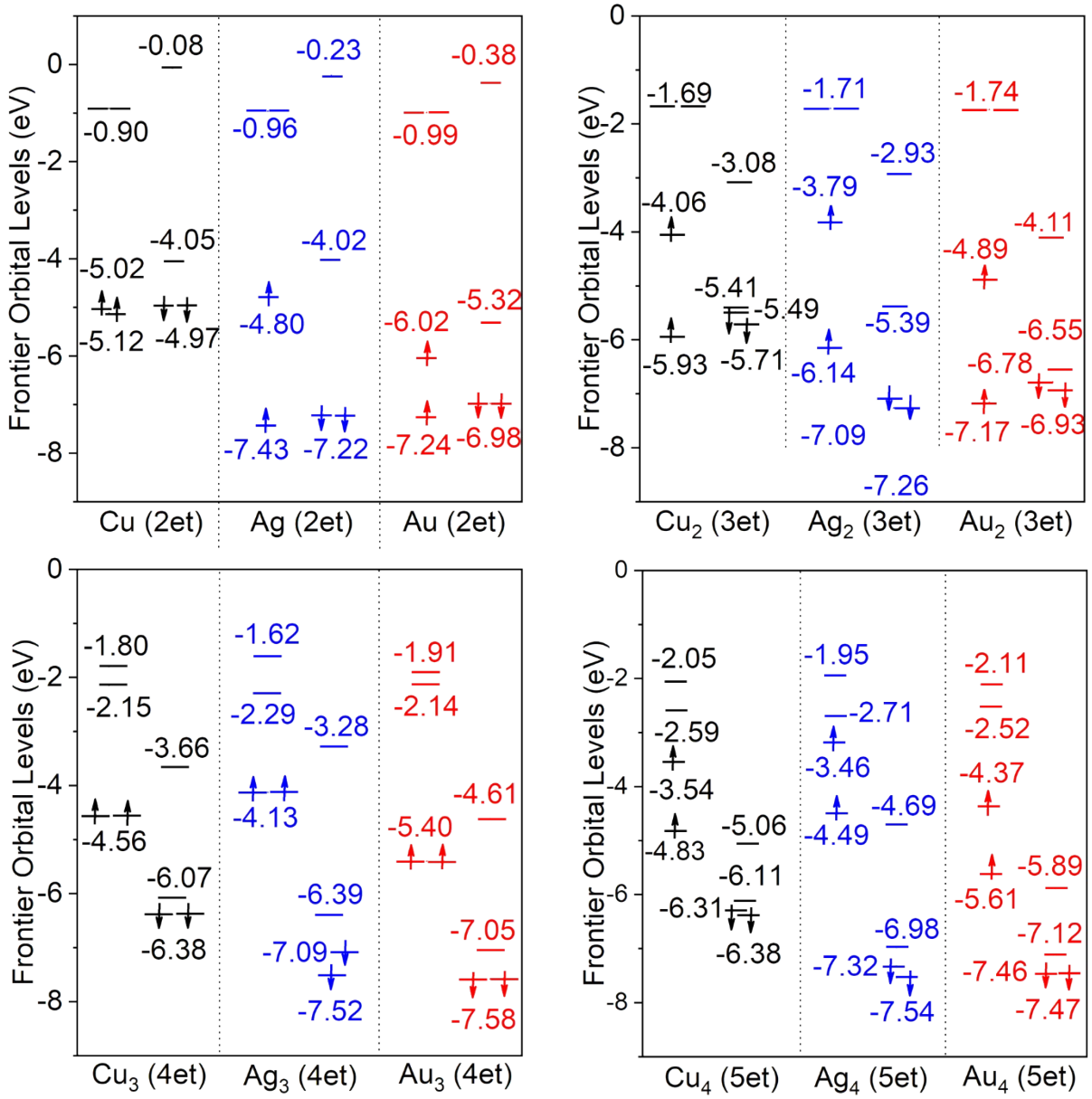

Figure S16. Energy levels of frontier orbitals of X_n clusters, where the geometry of X_n cluster was taken to be the same as that of nX/Ni(111)^P at the PBE/SDD level.

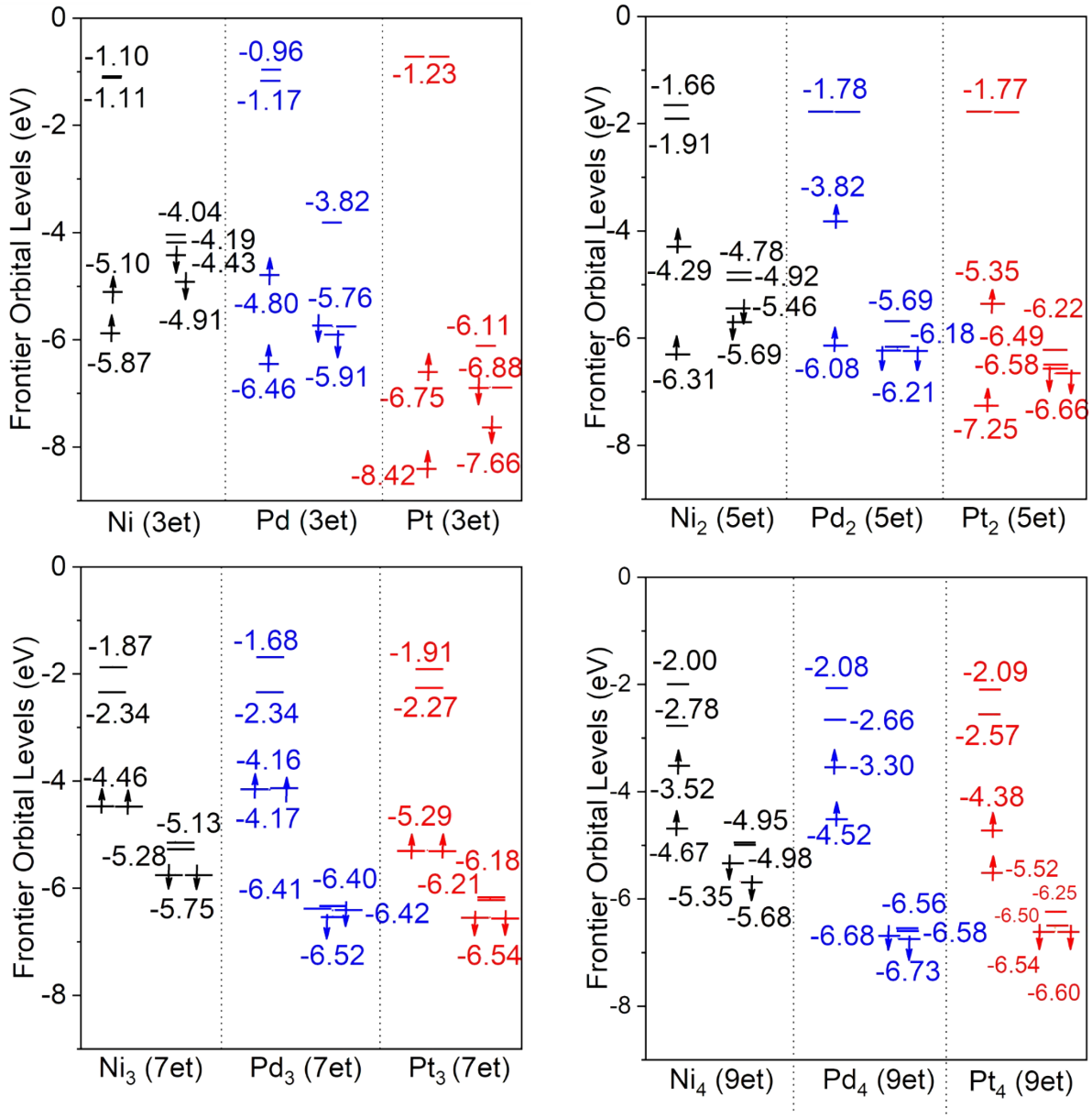

Figure S17. Energy levels of frontier orbitals of X_n clusters, where the geometry of X_n cluster was taken to be the same as that of nX/Cu(111)^P at the PBE/SDD level.

12. Adsorption sites, adsorption energy, and the Bader charge of CO adsorbed to the surfaces of M(111) and nX/M(111)

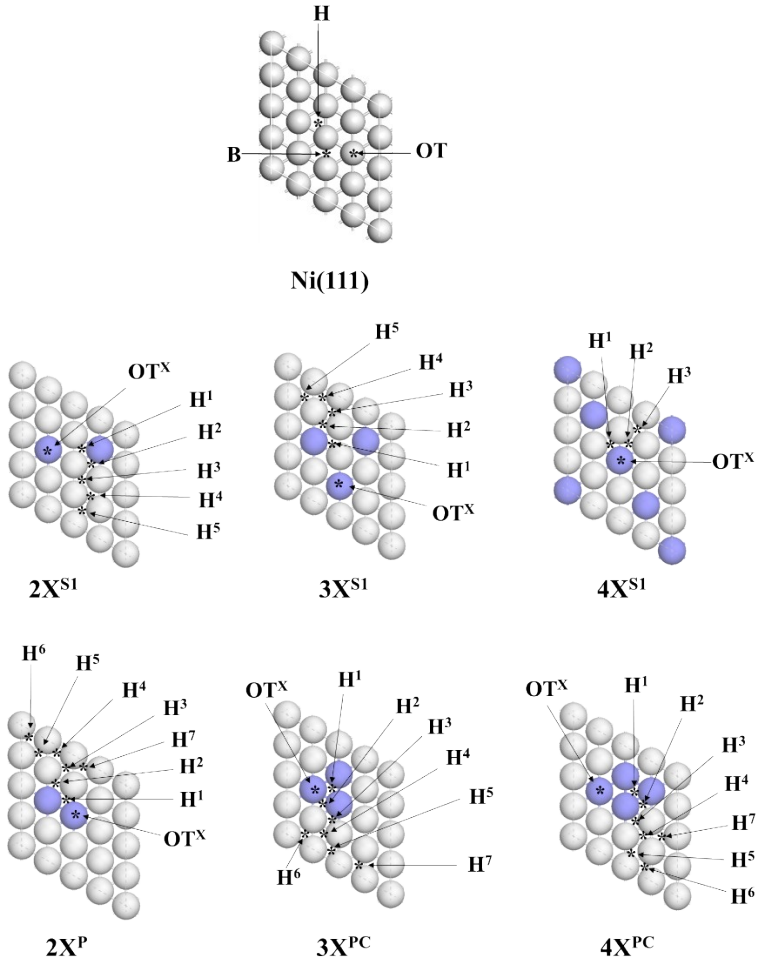

Scheme S5. The definition of various H sites for CO adsorption to the nX/Ni(111) (n = 0 ~ 4) surfaces

Table S10. The CO adsorption energy (eV) at the hollow (H), bridge (B), and on-Top (OT) sites on M(111)

	H	B	OT
Ni(111)	-1.92	-1.79	-1.56
Cu(111)	-0.95	-0.87	-0.78
Pd(111)	-2.03	-2.03	-1.43

Pt(111)	-1.88	-1.84	-1.77

Table S11. The CO adsorption energy (eV) at the several important sites on nX/Ni(111) shown in Scheme S5

Alloys	Sites						
$2X^{S1}$	H^1	H^2	H^3	H^4	H^5		
X = Cu	Change to B	Change to H^3	-1.93	-1.92	-1.91		
X = Ag	Change to B	Change to H^3	-1.83	-1.85	-1.86		
X = Au	Change to B	Change to H^3	-1.82	-1.87	-1.88		
$3X^{S1}$	H^1	H^2	H^3	H^4	H^5		
X = Cu	Change to B	Change to B	-1.93	-1.92	-1.91		
X = Ag	Change to B	Change to H^3	-1.83	-1.82	-1.85		
X = Au	Change to B	Change to H^3	-1.79	-1.77	-1.86		
$4X^{S1}$	H^1	H^2	H^3				
X = Cu	Change to B	Change to H^3	-1.95				
X = Ag	Change to B	Change to H^3	-1.79				
X = Au	Change to B	Change to H^3	-1.70				
$2X^{P}$	H^1	H^2	H^3	H^4	H^5	H^6	H^7
X = Cu	Change to T	Change to H^3	-1.93	-1.90	-1.92	-1.90	
X = Ag	Change to T	Change to H^3	-1.83	-1.85	-1.86	-1.82	
X = Au	Change to H^7	Change to H^3	-1.82	-1.86	-1.89	-1.85	-1.86
$3X^{PC}$	H^1	H^2	H^3	H^4	H^5	H^6	H^7
X = Cu	-0.90	Change to T	Change to H^4	-1.95	-1.92	-1.91	-1.94
X = Ag	-0.24	Change to T	Change to H^4	-1.84	-1.86	-1.86	-1.84
X = Au	-0.27	Change to H^5	Change to H^4	-1.77	-1.84	-1.85	-1.75
$4X^{PC}$	H^1	H^2	H^3	H^4	H^5	H^6	H^7
X = Cu	-0.93	Change to T	Change to H^4	-1.94	-1.90	-1.94	
X = Ag	-0.26	Change to T	-1.82	-1.82	-1.84	-1.82	
X = Au	-0.28	Change to H^7	Change to H^3	-1.73	-1.82	-1.73	-1.83

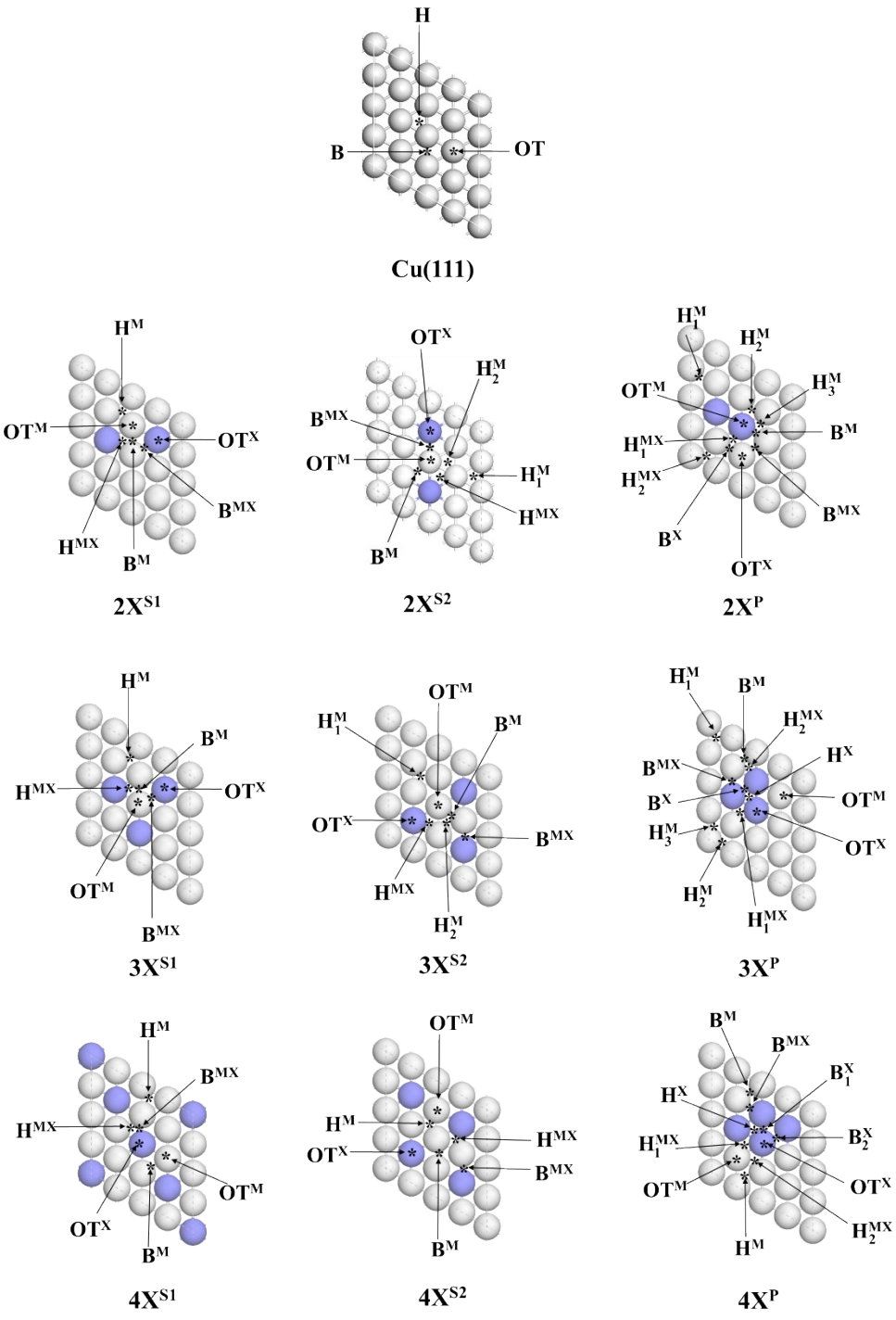

Scheme S6. The CO adsorption sites on the Cu(111) and nX/Cu(111) surfaces

Table S12. The CO adsorption energy (eV) at the several important sites on the nX/Cu(111) surfaces shown in Scheme S6

$2X^{S1}$	H^{M}	B^{M}	OT^{M}	H^{MX}	B^{MX}	OT^{X}	
X = Ni	-0.85	\[a)]	-0.87	\	\	-1.70	
X = Pd	-0.79	\	\	-1.02	-1.00	-1.15	
$2X^{S2}$	H_1^{M}	H_2^{M}	B^{M}	OT^{M}	H^{MX}	B^{MX}	OT^{X}
X = Pt	-0.85	-0.72	\	-0.56	\	\	-1.51
$2X^{P}$	H_1^{M}	H_2^{M}	H_3^{M}	H_1^{MX}	H_2^{MX}	B^{X}	OT^{X}
X = Ni	-0.47	-0.48	-0.46	\	\	-1.48	-1.43
X = Pd	-0.82	-0.84	\	-1.28	-1.03	-1.29	-1.14
X = Pt	-0.71	-0.85	\	\	\	-1.43	-1.43
$3X^{S1}$	H^{M}	B^{M}	OT^{M}	H^{MX}	B^{MX}	OT^{X}	
X = Ni	-0.87	OT^{X}	-0.67	To OT^{X}	To OT^{X}	-1.69	
X = Pd	-0.80	H^{MX}	-0.61	-1.00	-0.97	-1.14	
$3X^{S2}$	H_1^{M}	H_2^{M}	OT^{M}	H^{MX}	B^{MX}	OT^{X}	
X = Pt	-0.83	-0.64	-0.54	To OT^{X}	To OT^{X}	-1.50	
$3X^{PC}$	H_1^{M}	H_2^{M}	H_3^{M}	H^{X}	B^{X}	OT^{X}	
X = Ni	-0.86	-0.85	-0.86	-2.16	H^{X}	-1.67	
X = Pd	-0.79	-0.79	-0.79	-1.48	H^{X}	-1.12	
X = Pt	/	-0.80	-0.75	-1.43	-1.43	-1.37	
$4X^{S1}$	H^{M}	B^{M}	OT^{M}	H^{MX}	B^{MX}	OT^{X}	
X = Ni	-0.87	To OT^{X}	-0.70	/	/	-1.70	
X = Pd	-0.77	/	-0.84	-1.01	-0.97	-1.13	
$4X^{S2}$	H^{M}	B^{M}	OT^{M}	H^{MX}	B^{MX}	OT^{X}	
X = Pt	-0.64	/	-0.55	/	/	-1.48	
$4X^{PC}$	H^{M}	H^{X}	H_2^{MX}	B_2^{X}	OT^{X}		
X = Ni	-0.87	-2.14	/	/	/		
X = Pd	-0.76	-1.47	-1.04	-1.28	-1.11		

X = Pt	-0.72	-1.36	/	-1.31	-1.31

[a] Adsorptions of CO at these sites were not calculated.

Table S13. The adsorption energy ($E_{ads(CO)}$ in eV) and C-O bond stretching vibration frequency ($\nu_{(C-O)}$ in cm^{-1}) of CO at the hollow site of Ni(111) and Cu(111)

Models	$E_{ads(CO)}$	the functional used	the model size	Ref.
Ni(111)	-1.92 eV	PBE	p(4x4)	[This work]
	-1.92 eV	PBE	p(3x3)	[ref. S1]
	-1.90 eV	PBE	p(3x3)	[ref. S2]
	-1.89 eV	PBE	p(2x4)	[ref. S3]
	-1.86 eV	PBE	p(2x2)	[ref. S4]
Cu(111)	-0.95 eV	PBE	p(4x4)	[This work]
	-0.87 eV	PBE	p(2x4)	[ref. S5]
	-0.86 eV	PW91	p(3x3)	[ref. S6]
	-0.78 eV	PW91	p(3x3)	[ref. S7]

Models	$\nu_{(C-O)}$	Ref.
Ni(111)	1759 cm^{-1}	[This work]
	~1850 cm^{-1} (large coverage)	[Exp. Ref. S8]
	~1816 cm^{-1} (small coverage)	[Exp. Ref. S9]
$4Au/Ni(111)^S$	1774 cm^{-1}	[This work]
Ni-based Au alloy	1862 cm^{-1} (large coverage)	[Exp. Ref. S8]
Cu(111)	1805 cm^{-1}	[This work]
	1814 cm^{-1} (small coverage)	[ref. S10]

REFERENCES

[S1] Zhu, Y.-A.; Chen, D.; Zhou, X.-G.; Yuan, W.-K. DFT studies of dry reforming of methane on Ni catalyst. *Catal. Today*, **2009**, *148*, 260–267.

[S2] Carrasco, J.; Barrio, L.; Liu, P.; Rodriguez, J.; Ganduglia-Pirovano, M. V. Theoretical studies of the adsorption of CO and C on Ni(111) and $Ni/CeO_2(111)$: evidence of a strong metal−support interaction. *J. Phys. Chem. C*, **2013**, *117*, 8241−8250.

[S3] Guo, X.; Liu, H.; Wang, B.; Wang, Q.; Zhang, R. Insight into C + O(OH) reaction for carbon elimination on different types of CoNi(111) surfaces: a DFT study. *RSC Adv*., **2015**, *5*, 19970.

[S4] Liu, H.; Zhang, R.; Ding, F.; Yan, R.; Wang, B.; Xie, K. A first-principles study of C + O reaction on NiCo(111) surface. *Appl. Surf. Sci.,* **2011**, *257*, 9455– 9460.

[S5] Stroppa, A.; Termentzidis, K.; Paier, J.; Kresse, G.; Hafner, J. CO adsorption on metal surfaces: A hybrid functional study with plane-wave basis set. *Phys. Rev. B*, **2007**, *76*, 195440.

[S6] Grabow, L. C.; Mavrikakis, M. Mechanism of methanol synthesis on Cu through CO_2 and CO hydrogenation. *ACS Catal*. **2011**, *1*, 365–384.

[S7] Wang, Y.-X.; Wang, G.-C. A Systematic theoretical study of water gas shift reaction on Cu(111) and Cu(110): potassium effect. *ACS Catal*. **2019**, *9*, 2261−2274.

[S8] Beniya, A.; Ikuta, Y.; Isomura, N.; Hirata, H.; Watanabe, Y. Synergistic promotion of NO-CO reaction cycle by gold and nickel elucidated using a well-defined model bimetallic catalyst surface. *ACS Catal.* **2017**, *7*, 1369−1377.

[S9] Smirnov, K. S.; Raseev, G. Coverage dependent IR frequency shift of CO molecules adsorbed on Ni (111) surface. *Surf. Sci*. **1997**, *384*, 875−879.

[S10] Hayden, B. E.; Kretzschmar, K.; Bradshaw, A. M. An infrared spectroscopic study of CO on Cu(111): The linear, bridging and physisorbed species. *Surf. Sci.* **1985**, *155*, 553-566.